Programmed genome editing of the omega-1 ribonuclease of the blood fluke, *Schistosoma mansoni*

Wannaporn Ittiprasert[1], Victoria H. Mann[1], Shannon E. Karinshak[1], Avril Coghlan[2], Gabriel Rinaldi[2], Geetha Sankaranarayanan[2], Apisit Chaidee[1,3], Toshihiko Tanno[4], Chutima Kumkhaek[5], Pannathee Prangtaworn[1,6], Margaret Mentink-Kane[7], Christina J. Cochran[1], Patrick Driguez[2], Nancy Holroyd[2], Alan Tracey[2], Rutchanee Rodpai[1,3], Bart Everts[8], Cornelis H. Hokke[8], Karl F. Hoffmann[9], Matthew Berriman[2], Paul J. Brindley[1]

1. Department of Microbiology, Immunology & Tropical Medicine, & Research Center for Neglected Diseases of Poverty, School of Medicine & Health Sciences, George Washington University, Washington, D.C. 20037, USA

2. Wellcome Sanger Institute, Wellcome Genome Campus, Hinxton, CB10 1SA, UK

3. Department of Parasitology, Faculty of Medicine, Khon Kaen University, Khon Kaen, 40002, Thailand

4. Department of Surgery and the Institute of Human Virology, University of Maryland, Baltimore, MD 21201, USA

5. Cellular and Molecular Therapeutics Laboratory, National Heart, Lungs and Blood Institute, National Institutes of Health, Bethesda, MD 20814 USA

6. Department of Parasitology, Faculty of Medicine Siriraj Hospital, Mahidol University, Bangkok, Thailand 10700

7. Schistosomiasis Resource Center, Biomedical Research Institute, Rockville, MD 20850, USA

8. Department of Parasitology, Leiden University Medical Center, Leiden, Netherlands

9. Institute of Biological, Environmental & Rural Sciences (IBERS), Aberystwyth University, Aberystwyth, SY23 3DA, UK

Running title; **Genome editing of schistosome omega-1**

Keywords: *Schistosoma mansoni*; genome editing; CRISPR/Cas9; omega1; ribonuclease; flatworms; Platyhelminthes; functional genomics; lentivirus; homology directed repair; non-homologous end joining; double stranded break; Th2 phenotype; monocytic macrophage cell; granuloma; schistosomiasis

*Correspondence, Paul Brindley, pbrindley@gwu.edu

Abstract

CRISPR/Cas9 based genome editing has yet been reported in parasitic or indeed any species of the phylum Platyhelminthes. We tested this approach by targeting omega-1 (ω1) of *Schistosoma mansoni* as a proof of principle. This secreted ribonuclease is crucial for Th2 priming and granuloma formation, providing informative immuno-pathological readouts for programmed genome editing. Schistosome eggs were either exposed to Cas9 complexed with a synthetic guide RNA (sgRNA) complementary to exon 6 of ω1 by electroporation or transduced with pseudotyped lentivirus encoding Cas9 and the sgRNA. Some eggs were also transduced with a single stranded oligodeoxynucleotide donor transgene that encoded six stop codons, flanked by 50 nt-long 5'- and 3'-microhomology arms matching the predicted Cas9-catalyzed double stranded break (DSB) within ω1. CRISPResso analysis of amplicons spanning the DSB revealed ~4.5% of the reads were mutated by insertions, deletions and/or substitutions, with an efficiency for homology directed repair of 0.19% insertion of the donor transgene. Transcripts encoding ω1 were reduced >80% and lysates of ω1-edited eggs displayed diminished ribonuclease activity indicative that programmed editing mutated the ω1 gene. Whereas lysates of wild type eggs polarized Th2 cytokine responses including IL-4 and IL-5 in human macrophage/T cell co-cultures, diminished levels of the cytokines followed the exposure to lysates of ω1-mutated schistosome eggs. Following injection of schistosome eggs into the tail vein of mice, the volume of pulmonary granulomas surrounding ω1-mutated eggs was 18-fold smaller than wild type eggs. Programmed genome editing was active in schistosomes, Cas9-catalyzed chromosomal breakage was repaired by homology directed repair and/or non-homologous end joining, and mutation of ω1 impeded the capacity of schistosome eggs both to drive Th2 polarization and to provoke formation of pulmonary circumoval granulomas. Knock-out of ω1 and the impaired immunological phenotype showcase the novel application of programmed gene editing in and functional genomics for schistosomes.

58 **Introduction**

59 Schistosomiasis is considered the most problematic of the human helminth diseases in terms of
60 morbidity and mortality (1-4). The past decade has seen major advances in knowledge and
61 understanding of the pathophysiology, developmental biology, evolutionary relationships and
62 genome annotation of the human schistosomes (5-16). Establishing CRISPR/Cas9 genome
63 editing in schistosomiasis would greatly enable effective functional genomics approaches. The
64 stable CRISPR/Cas9-based site-specific gene mutation and phenotyping will drive innovation
65 and a deeper understanding of schistosome pathogenesis, biology and evolution (17).

66 The schistosome egg plays a central role both in disease transmission and pathogenesis (1). The
67 appearance of *S. mansoni* eggs in host tissues by six to seven weeks after infection coincides
68 with profound polarization to a granulomatous, T helper type 2 (Th2) cell phenotype (18-22).
69 Numerous egg proteins have been characterized, with >1,000 identified in a well-studied fraction
70 termed soluble egg antigen (SEA) (23-26). In viable eggs, about 30 of the SEA proteins are
71 located outside the developing miracidium and encompass the complement of secreted antigens
72 (egg-secreted proteins, ESP) that interact with host tissues to facilitate the passage of the egg
73 from the mesenteric veins to the intestinal lumen (27). The T2 ribonuclease omega-1 (ω1) is the
74 principal Th2-inducing component of ESP with its Th2-polarizing activity dependent upon both
75 its RNase activity and glycosylation (19, 20, 28). This RNase is hepatotoxic (29), and its
76 secretion by eggs into the granuloma regulates the pattern recognition receptor signaling
77 pathways in dendritic cells that, in turn, prime Th2 responses from $CD4^+$ T cells (30). Secreted
78 ω1 provokes granulomatous inflammation around eggs traversing the wall of the intestines, and
79 trapped in hepatic sinusoids and other host organs, driving fibrosis that eventually results in
80 hepatointestinal schistosomiasis (1, 31).

81 As ω1 drives distinctive immunological phenotypes including Th2 polarization and granuloma
82 formation, we investigated, for the first time in schistosomes and indeed any flatworms, the use
83 of programmed CRISPR/Cas9-mediated genome editing (32, 33) to alter the ω1 locus by both
84 gene knockout and knock-in approaches. The investigation revealed that programmable genome
85 editing catalyzed by the bacterial endonuclease Cas9 was active in schistosomes, with
86 chromosomal double stranded breaks (DSB) repaired by homology directed repair (HDR) using
87 a donor, single stranded oligonucleotide template bearing short homology arms and/or by non-
88 homologous end joining (NHEJ). The programmed mutagenesis decreased levels of ω1 mRNA
89 and induced distinct *in vitro* and *in vivo* phenotypes, including a substantial loss of capacity of
90 SEA from ω1-mutated eggs to polarize Th2 cytokine responses (IL-4 and IL-5) in co-cultured
91 monocytic and T cells and loss of capacity to provoke formation of pulmonary granulomas *in*
92 *vivo*. Functional knock-out of ω1 and the resulting immunologically impaired phenotype
93 showcase the novel application of CRISPR/Cas9 and its utility for functional genomics in
94 schistosomes.

95 **Results**

96 ***Omega-1*, a multicopy locus on chromosome 1 of *S. mansoni* specifically expressed in eggs**

97 Five genomic copies of *ω1* were identified in the *S. mansoni* reference genome, version 5 (Fig.
98 s1) although the gene repetition at the ω1 locus on chromosome 1 presents a challenge for

genome assembly. A single copy of ω1 selected for genome editing, Smp_193860, included nine exons separated by eight introns and spanned 6,196 nt (Fig. 1a). Several other copies shared similar exon/intron structure and conserved coding sequences (Figs. s1, s2). The predicted coding sequence (CDS) of Smp_193860 encoded a ~27 kDa protein, of similar mass to the 31 kDa reported for ω1 (34). The gene encodes a secreted ribonuclease of the T2 family of transferase-type endoribonucleases with conserved catalytic regions (35). We designed a sgRNA targeting residues 3808 to 3827 within exon 6 of Smp_193860, adjacent to a AGG protospacer adjacent motif (PAM) and with the predicted Cas9 cleavage site located at three residues upstream of the PAM. (Figure s2 provides the nucleotide sequence of the Smp_193860 copy, and indicates the UTR, coding exons and introns; 6,196 nt.) The AGG and the nucleotide sequence complementary to this sgRNA were also present in the Smp_179960 and Smp_184360 copies of ω1. These three copies shared >99% identity although the CDS of each differed by several substitutions (Fig. s3a-c). All three copies of the *ω1* display a tight profile of developmental stage expression: expression is restricted to the mature egg, and with expression not apparent elsewhere during the developmental cycle of this schistosome (Fig. s1c) (36).

Homology Directed Repair and Non-Homologous End Joining pathways in schistosomes

The draft genome of *Schistosoma mansoni* was surveyed for key proteins of the non-homologous end joining (NHEJ) and homology directed repair (HDR) pathways. Artemis and DNA-PKcs are essential NHEJ factors in vertebrates (37-39). Candidate homologues for six of seven human NHEJ pathway genes and for two key HDR pathway genes, were identified by searching for matches to Pfam (Table s1). A putative homologue of Cernunnos/XLF was not apparent in *S. mansoni* (38) based on searching for the Pfam XLF domain (PF09302) found in human Cernunnos/XLF. The domain appears to be absent from all flatworm species studied by the International Helminth Genomes Consortium (40).

Site-specific integration of transgene confirmed CRISPR-Cas9 activity in schistosomes

The activity and efficiency of CRISPR/Cas9 to edit the schistosome genome, by targeting the ω1 locus, was explored using two approaches. First, a ribonucleoprotein complex (RNP) comprised of sgRNA mixed with recombinant Cas9 endonuclease was delivered into schistosome eggs isolated from livers of experimentally-infected mice (eggs termed 'LE', 'liver eggs') by electroporation. In addition, Homology Directed Repair (HDR) of CRISPR/Cas9-induced double stranded breaks (DSBs) at the ω1 locus in the presence of a donor DNA template was investigated (41-43). A single stranded oligodeoxynucleotide (ssODN) of 124 nt in length was delivered to some LE as a template for HDR of chromosomal DSBs (Fig. 1b). The ssODN included a short transgene encoding six stop codons flanked by 5'- and 3'-homology arms, each arm 50 nt in length, complementary to the genome sequence of exon 6 on the 5′ and 3′ sides of the Cas9 cleavage site (Figs. 1a, 1b). In a second approach, a lentivirus vector (pLV-ω1X1; Fig. 1c) that included Cas9, driven by the mammalian translational elongation factor 1 promoter, and the exon 6-targetting sgRNA (20 nt), driven by the human U6 promoter was engineered (44). LE were transduced with pseudotyped lentiviral virions (LV) by exposure in culture to LV for 24 hours (45) and, thereafter, transfected with the ssODN repair template. In both approaches, expression of ω1 in LE after 72 hours in culture was ascertained.

140 Given that the donor ssODN included a short transgene that facilitates genotyping, PCR was
141 performed using template genomic DNAs from the CRISPR/Cas9-treated LE (41) to reveal the
142 site-specific knock-in (KI). A forward primer termed Smω1X1-6stp-cds-F specific for the
143 ssODN transgene was paired with three discrete reverse primers, termed Smω1-R1, Smω1-R2
144 and Smω1-R3, at increasing distance from the predicted HDR insertion site in ω1 (Table s2).
145 Amplicons of the expected sizes of 184, 285 and 321 nt were observed in genome-edited eggs
146 but not in control eggs (Fig. 2a, b; Fig. s4a), a diagnostic pattern indicative of the ssODN
147 transgene insertion into ω1 and, in turn, indicating that the resolution of the DSB at the ω1 locus
148 from CRISPR/Cas9 had been mediated by HDR. Amplification using a control primer pair that
149 spanned the predicted DSB, termed Smω1-control-F/R, yielded control amplicons of the
150 expected 991 nt. Similar findings were observed with genome editing delivered by RNPs and by
151 LV (Fig. s4). Sanger sequence analysis of the knocked-in amplicons (KI-R1, KI-R2 and KI-R3)
152 confirmed the presence of the transgene inserted into the ω1 locus at the site predicted for
153 programmed Cas9 cleavage (Fig. 2c).

154 **Programmed mutations in exon 6 of ω1**

155 The activity of CRISPR/Cas9 was first evaluated by a quantitative PCR (qPCR) approach that
156 relies on the inefficient binding of a primer overlapping the gRNA target, i.e. where mutations
157 are expected to have occurred, compared to the binding efficiency of flanking primers, i.e.
158 outside the mutated region (46, 47). The overlapping (OVR) primer pair shared the reverse
159 primer with OUT primer (Fig. s5a). Genomic DNA template was used for qPCR to quantify the
160 efficiency of CRISPR-mediated mutagenesis at the target locus; the ratio between the OVR
161 products and OUT products estimate the relative fold amplification reduction in CRISPR/Cas9-
162 manipulated samples compared to controls in the target sequence of the gRNA, i.e. the annealing
163 site for the OVR primer. Relative fold amplification was reduced by 12.5% in gDNA isolated
164 from eggs treated with pLV-ω1X1 and ssODN whereas a reduction in relative fold amplification
165 of 2.5, 6.9, and 4.5 were observed in eggs treated with gRNA/Cas9 RNP complex alone,
166 gRNA/Cas9 RNP complex and ssODN, or pLV-ω1X1 alone, respectively. A reduction in
167 relative fold amplification was not apparent among control groups, i.e. untreated eggs, eggs
168 electroporated in the presence of Opti-MEM only, Cas 9 only, eggs transduced with heat-
169 inactivated pLV-ω1X1 with ssODN donor, and eggs transfected with ssODN only (Fig. s5b).

170 To further characterize and quantify the mutations that arose in the genome of *ω1* gene-edited
171 eggs, we used an amplicon-sequencing approach. Barcoded amplicon libraries were constructed
172 from pooled genomic DNA of six independent exposures of LE to pLV-ω1X1 and the donor
173 ssODN. Each amplicon was sequenced on the MiSeq Illumina platform and the CRISPResso
174 pipeline (48) was used to analyze deep-coverage sequence. More than 56 million sequenced
175 reads were compared to the reference sequence of the Smp_193860 locus (Table s3), which
176 revealed that 71% exhibited the wild type (WT; i.e., unmodified DNA) whereas 29 % reads
177 exhibited apparent mutations (Fig. 2d) across the 202 bp amplicon, with 0.13% insertions, 0.58%
178 deletions and 28.2% substitutions (Table s3, sample 9). In contrast, in the control eggs-only
179 group, 76% were WT, and 24% of reads exhibited apparent mutations, with 0.14% insertions,
180 0.33% deletions, and 24.0% substitutions (Fig. 2e, sample 2 in Table s3). Thus, subtracting the
181 rate of apparent mutations in the control, we estimated that 0.25% and 4.2% of reads in the
182 experimental sample carried programmed CRISPR-induced deletions and substitutions,

183 respectively. Indels of 1-2 bp, or multiples thereof, in coding DNA cause frame-shifts, and
184 consistent with its higher rate of indels, the CRISPR/Cas9-treated sample displayed a higher rate
185 of frame-shifts compared to a sample from control eggs, 2.0 % versus 1.4 %) (Table s3).

186 Many apparent sequence variants common to the control and edited eggs likely reflect
187 polymorphism among copies of ω1 rather than programmed mutations. The sequence reads
188 revealed several common variants, such as adjacent 'TA' substitutions instead of 'CC' at
189 positions 152-153 of the amplicon, which encodes a change from Q to K at the amino acid level.
190 The gene Smp_193860 has 'TA' at this position in the V5 assembly (12), as does the mRNA
191 XP_018647487.1 from the NCBI database, whereas Smp_193860, Smp_184360 and
192 Smp_179960 all have 'CC' at this position in the V7 assembly (Berriman and co-workers, in
193 preparation) (Fig. s3 a, b), whereas 'CC' was also observed in KI fragments by Sanger direct
194 sequencing (Fig. 2c). A second common dinucleotide substitution from 'AC' to 'TT' at positions
195 60-61 encodes an amino acid change from T to F. Both dinucleotide substitutions occurred
196 together in 8% of reads in the control group (Table s3, sample 2,) and 4% of reads in the gene-
197 edited group (Table s3, sample 9). These non-synonymous substitutions may have functional
198 significance given their proximity to the catalytic site of the ribonuclease (Fig. s3c).

199 Along with the predicted NHEJ-catalyzed mutations, CRISPResso determined the rate of HDR-
200 mediated ssODN knock-in (Table s3; Fig. 2f). Here, insertion of the 24 bp transgene was
201 confirmed in 0.19% of the reads at the sgRNA programmed CRISPR/Cas9 target site (Fig. 2f;
202 sample 9 in Table s3). Some reads containing the knock-in sequence included the 'CC' to 'TA'
203 substitutions at positions 152-153 and 'AC' to 'TT' at positions 60-61 (Fig. s3; Table s3). This
204 indicates that the indels catalyzed by NHEJ and/or KI by HDR occurred in multiple copies of ω1
205 including Smp_193860, Smp_184360 and Smp_179960, and possibly also further copies not yet
206 annotated in the reference genome. The qPCR approach estimated a reduction by 12.5% in
207 relative fold amplification in the pLV-ω1X1 with ssODN treatment group (Fig. s5) whereas
208 CRISPResso analysis of the pooled NGS reads indicated a frequency of indel/substitution
209 mutation of ~4.5% (Table s3).

210 **Programmed gene editing markedly diminished the expression of ω1**

211 Liver eggs (LE) transfected with RNP complexes, without or with ssODN, displayed a down
212 regulation of the ω1-specific transcript of ~45% and 81%, respectively, compared to controls (p
213 ≤ 0.05; $n = 11$). However, LE transduced with pLV-ω1X1 virions, without or with ssODN,
214 showed a reduction of the *ω1*-specific transcripts of 67% and 83% respectively, when compared
215 to controls (Fig. 3a). Similar outcomes were seen in all biological replicates undertaken (n =11).
216 This outcome indicated that resolution of chromosomal DSB by NHEJ plus HDR provided
217 enhanced programmed gene knockout compared to NHEJ-mediated chromosomal repair alone.
218 Nevertheless, both RNPs and pLV virions efficiently delivered programmed gene editing to
219 schistosomes but lentiviral transduction delivered enhanced performance with stronger gene
220 silencing, in particular when the donor repair template was provided (Fig. 3a). When examined
221 at later time points (days 5 and 7 following manipulation of the LE), further reduction in ω1
222 abundance was not apparent (Fig. 3b).

223 Large DNA deletions have been associated with CRISPR/Cas9 mutations in another helminth
224 species (42). However, using qPCR to estimate relative copy number, as previously described

225 (49), evidence that silencing of *ω1* was associated with a reduction in the copy number of this
226 multi-gene locus was not seen (Fig. s6).

227 **Diminished ribonuclease activity in CRISPR/Cas9-mutated schistosome eggs**

228 The ribonuclease activity of the ω1 glycoprotein in SEA is associated with the Th2-polarized
229 immune response that underpins the appearance of schistosome egg granulomata (19, 22).
230 Ribonuclease activity of SEA from control and experimental groups on substrate yeast RNA was
231 investigated following CRISPR/Cas9 programmed mutation of ω1 mediated by the RNP and the
232 pseudotyped lentiviral approaches with or without ssODN (20, 50). Intact yeast RNA was
233 evident in the DNase-RNase free condition (negative control), indicative of absence of RNase
234 activity in the reagents (200 ng yeast RNA at the outset). There was near complete hydrolysis of
235 yeast RNA following exposure to RNase A (positive control); ~1.4 ng of RNA remained intact.
236 Wild type SEA exhibited marked RNase activity against the yeast RNA; ~70 ng RNA remained
237 intact after one hour, corresponding to >60% digestion. Incubation of the RNA with Δω1-SEA
238 from the experimental groups, RNP, RNP + ssODN, pLV-ω1X1, and pLV-ω1X1+ssODN,
239 resulted in ~30% substrate digestion, with 124, 140, 135 and 153 ng of RNA remaining,
240 respectively. All conditions for programmed genome editing resulted in less digestion of the
241 yeast RNA than for wild type SEA ($p \leq 0.0001$) (Figs. 3c, 3d). Moreover, the Δω1-SEA with
242 programmed knock-in exhibited less RNase activity than Δω1-SEA prepared without the donor
243 ssODN repair template ($p \leq 0.01$).

244 **Depleting SEA of ω1 down-regulated Th2 response**

245 The ω1 ribonuclease alone is capable of conditioning human monocyte-derived dendritic cells to
246 drive Th2 polarization (22) and enhanced $CD11b^+$ macrophage modulation of intracellular toll
247 like receptor (TLR) signaling (30). Ribonuclease ω1 inhibited TLR-induced production of IL-1β
248 and redirected the TLR signaling outcome towards an anti-inflammatory posture via the mannose
249 receptor (MR) and dectin (22, 51, 52). The human monocytic cell line, THP-1, and the Jurkat
250 human $CD4^+$ T cell line were employed to investigate the interaction of antigen presenting cells
251 and T cells (53, 54). At the outset, the THP-1 cells were differentiated to macrophages for 48
252 hours, then pulsed with SEA or Δω1–SEA for 48 hours, after which the Jurkat $CD4^+$ T cells were
253 added to the wells. Subsequently, the co-culture continued for 72 hours. Representative
254 cytokines, including IL-4, IL-5, IL-13, IL-2, IL-6, IL-10, TNF-α and IFN-γ, were quantified in
255 supernatants of the co-cultures (Fig. 4). SEA from ω1-mutated eggs induced reduced levels of
256 Th2 cytokines, including IL-4 and IL-5, in comparison to wild type SEA ($p \leq 0.01$), and a trend
257 towards less IL-13 production was also observed (Fig. 4). Moreover, reduced levels of IL-6 and
258 TNF-α were observed ($p \leq 0.01$). By contrast, significant differences in levels of IL-10 and IL-2
259 were not evident between the WT- and mutant-SEA groups. IFN-γ was not detected following
260 pulsing with the WT-SEA or mutant-SEA (Fig. s7).

261 **Granulomatous inflammation markedly reduced in lungs of mice injected with Δω1 eggs**

262 Following the entrapment of eggs in the intestines, liver and eventually lungs, the glycosylated
263 ω1 ribonuclease represents the principal stimulus that provokes the development of the
264 circumoval granuloma, necessary for extravasation of the eggs (55). A long-established model of
265 the schistosome egg granuloma employs tail vein injection of eggs into mice, which leads to

266 formation of circumoval granuloma in the mouse lung (56-58). The latter approach has been
267 extensively employed for immunopathogenesis-related studies of ω1 (16). Accordingly, to elicit
268 circumoval granulomas, ~3,000 WT or Δω1 LE were injected into the lateral vein of the tail of
269 BALB/c mice. The mice were euthanized 10 days after injection, and the entire left lung was
270 removed, fixed, sectioned, and stained for histological analysis (Fig. 5). Representative digital
271 microscopic images of the whole mouse lungs acquired through high-resolution 2D digital scans
272 are presented in Figure 5, panels a-g. At low magnification (2×), much more severe and
273 widespread inflammation was visible in lungs exposed to WT eggs compared to Δω1-eggs. In
274 addition, markedly more intense and dense focal inflammation was induced by WT compared to
275 Δω1-eggs (Fig. 5b). Granulomas were not seen in control naïve mice not exposed to schistosome
276 eggs (Fig. 5c). At 20× magnification, vast disparity in volume of the circumoval granulomas was
277 observed for WT versus Δω1 LE (Fig. 5a1-a2, 5d, 5e *vs.* Figs. 5b1-b2, 5f, 5g). The volume of
278 granulomas surrounding single schistosome eggs was quantified; those surrounding WT eggs in
279 lungs of the mice were 18-fold greater than for Δω1-eggs, $21\times10^{-2}\pm1.61\times10^{-3}$ mm^3 and 0.34×10^{-2}
280 $\pm0.12\times10^{-4}$ mm^3 (mean ± S.E., 17-26 granulomas per mouse), respectively ($p < 0.0001$) (Fig. 5h).
281 The experiment was repeated with 3-4 mice per group with a similar outcome. The findings
282 documented marked deficiency in the induction of pulmonary granulomas by the Δω1 compared
283 to WT eggs of *S. mansoni*.

284 **GenBank/EMBL/DDBJ**

285 ***Database accessions*** Sequence reads from the amplicon NGC libraries are available at the
286 European Nucleotide Archive, study accession number ERP110149. Additional information is
287 available at Bioproject PRJNA415471, https://www.ncbi.nlm.nih.gov/bioproject/PRJNA415471
288 and GenBank accessions SRR6374209, SRR6374210.

289 **Discussion**

290 Using *Schistosoma mansoni* as an exemplar, we have demonstrated the activity and feasibility of
291 programmed CRISPR/Cas9 genome editing in the phylum Platyhelminthes. On-target genome
292 editing was evidenced by site-specific mutations at the *ω1* locus on chromosome 1. The
293 chromosomal lesion was repaired by the non-homologous end joining (NHEJ) pathway (59) in
294 the absence of a donor oligonucleotide and by homology directed repair (HDR) when a single
295 stranded oligonucleotide donor template was provided (60-62).

296 To investigate the feasibility of genome editing, schistosome eggs were transfected with
297 ribonucleoprotein particle (RNP) complexes and with lentiviral virions carrying the
298 CRISPR/Cas9 components, in similar fashion to earlier reports in cell lines, tissues and entire
299 organisms (63-66). Delivery by RNPs facilitates immediate editing although the short half-life of
300 the RNP components may be disadvantageous. Delivery by plasmids and by viral-mediated
301 infection may provide sustained Cas9 activity, transgene integration in non-dividing cells, and
302 other advantages (33, 67). Transfection by LV provides a hands-free approach to enable scaling
303 of gene editing and the potential that less accessible and/or differentiated cells can be reached.
304 When released into the mesenteric veins from adult female, the schistosome ovum each contains
305 single celled zygote surrounded by 30 to 40 vitelline cells (27). By six days later, the miracidium
306 that has developed within the eggshell is a multi-cellular, mobile, ciliated larva comprised of
307 organs, tissues, muscles and nerves (25, 68-70).

308 To investigate the efficiency of programmed genome editing, several parallel approaches were
309 undertaken including NGS- and quantitative PCR-based analysis of pooled genomic DNAs,
310 analysis of levels of *ω1*-transcripts and ribonuclease, and immuno-phenotypic status of cultured
311 cells and of mice exposed to gene edited eggs. Analysis of the deep-coverage nucleotide
312 sequence reads of amplicons spanning the predicted DSB site in the *ω1* locus revealed that
313 ~4.5% of the reads were mutated by insertions, deletions, and substitutions. The target locus was
314 mutated by knock-in (KI) of a ssODN repair template bearing short homology arms to mediate
315 homology directed repair following DSB at *ω1*, with an efficiency for HDR of 0.19% insertion
316 of the donor transgene. Numerous substitutions in addition to deletions and insertions were seen,
317 although some may reflect single nucleotide polymorphisms (SNPs) among the multiple gene
318 copies rather than genome editing-induced changes. As well as the anticipated ease of access by
319 the RNPs, virions and the donor template ssODN to cells proximal to the eggshell compared to
320 the cells deeper within the egg, other factors may have contributed to variability of CRISPR
321 efficiency among the eggs and the cells within individual eggs. Given the multiple copies of *ω1*,
322 the numerous cells in the mature egg (68), the spectrum of development of the eggs in LE, and
323 other factors, a mosaic of mutations would be expected: some genomes to display HDR but not
324 NHEJ, some NHEJ but not HDR, others both NHEJ and HDR, and many to retain the wild type
325 genotype. HDR proceeds at cell division, with the cell at late S or G2 phase following DNA
326 replication where the sister chromatid serves as the repair template; otherwise, NHEJ proceeds to
327 repair the DSB (71).

328 Expression levels of *ω1* were diminished by as much as 83% relative to controls suggesting that
329 Cas9 catalyzed the mutation of *ω1*, and that programmed Cas9-induced DSBs had been resolved
330 by NHEJ and/or HDR. Knock-in of the ssODN repair template induced 81-83 % reduction in
331 ω1-specific mRNA levels, whereas down regulation of 45 to 67 % followed the exposure of eggs
332 to RNP or lentivirus without ssODN. Ribonuclease activity in *ω1*-mutated eggs was likewise
333 significantly diminished. Curiously, less than 5% efficiency (NGS findings) in gene editing
334 appeared to account for this markedly reduced (>80%) gene expression. The possibility of large-
335 scale deletions, as reported in *Strongyloides stercoralis* (42), presented an explanation for this
336 apparent paradox. However, analysis of copy number by qPCR failed to reveal apparent
337 differences for *ω1* among treatment and control groups of eggs. An alternative explanation for
338 the paradox may be the tight stage- and tissue-specific expression of ω1. Within the mature egg,
339 the fully developed miracidium is surrounded by a squamous, syncytial epithelium termed
340 variously as the envelope, the inner envelope, or von Lichtenberg's envelope (25, 27, 68, 69).
341 This layer is metabolically active (27) and is considered to be the site of synthesis of the ω1 T2
342 ribonuclease that is released from the egg into the granuloma (25, 27, 29), along with other
343 secreted/ excreted proteins that facilitate egress of the egg from the blood vessels and through the
344 wall of the intestine (27). Expression of ω1 is developmentally tightly regulated: based on
345 comparison of expression in the egg to expression in the miracidium, immunostaining and
346 transmission electron microscopy of the mature egg, and on meta-analysis of transcriptomic
347 findings, all or most expression of ω1 occurs solely in the mature egg; expression does not occur
348 in the immature egg or other developmental stages (20, 25, 27, 29, 72, 73) (Fig. s1c).The virions
349 may have transduced only a small number of the cells within the mature egg because, after entry
350 into the egg, the virus would be expected to contact the inner envelope, rather than traveling
351 further to the cells of the miracidium. Accordingly, the efficiency of gene editing may have
352 ranged from high to low through the cells of the egg due to ease of virus access, and displayed
353 highest efficiency in the cells of the inner envelope where ω1 is expressed. This may explain the

354 paradox involving >80% reduction in ω1-encoding transcripts in tandem with the <5% gene
355 editing efficiency.

356 To address the effects on the hallmark Th2 polarization of the immune response to
357 schistosomiasis (74), co-cultures of human macrophages and T cells were exposed to Δω1-SEA
358 and mice were exposed to Δω1-eggs. Whereas wild type SEA polarized Th2 cytokine responses
359 including IL-4 and IL-5 in the co-cultures, significantly reduced levels of these cytokines were
360 observed after exposure to ω1-mutated SEA. Moreover, following introduction of eggs into the
361 tail vein of mice, the volume of pulmonary circumoval granulomas around Δω1 eggs was
362 enormously reduced compared to those provoked by wild type eggs. Whereas this outcome
363 extends earlier findings using lentiviral transduction of eggs of *S. mansoni* to deliver microRNA-
364 adapted short hairpin RNAs aiming to silence expression of ω1 (16), the decrement in granuloma
365 volume was vastly more marked in the present study. In addition to incomplete disruption of all
366 copies of ω1, residual granulomas around the mutant eggs may be due to the presence of other
367 Th2-polarizing components within SEA that have recently been reported (75). Given that the T2
368 ribonuclease ω1 is the major type 2-polarizing protein among egg-secreted proteins (19, 20), our
369 findings of a phenotype characterized by the absence of or diminutive granulomas provide
370 functional genomics support to this earlier advance (22).

371 **Conclusions**

372 These findings confirmed that somatic genome editing of schistosome eggs led to functional
373 knockout of the ω1 T2 ribonuclease, and mosaicism of mutant and wild type cells. The genome-
374 edited eggs exhibited loss of function of ω1 but remained viable. Programmed mutation of ω1
375 using CRISPR/Cas9 not only achieved the aim of establishing the applicability of genome
376 editing for functional genomics of schistosomes but also demonstrated manipulation of a gene
377 expressed in the schistosome egg, the developmental stage central to the pathophysiology of
378 schistosomiasis. This study provides a blueprint for editing other schistosome genes, and those of
379 trematodes and platyhelminths at large. The challenge for future studies is now to deliver
380 pseudotyped virions and programmed genome editing to the schistosome germ line. Mutant
381 parasite lines derived following this protocol (11, 76) will enable more comprehensive
382 understanding of the pathogenesis of this neglected tropical disease and accelerate the discovery
383 of novel strategies for parasite control.

384 **Materials and Methods**

385 **Ethics statement**

386 Mice experimentally infected with *S. mansoni*, obtained from the Biomedical Research Institute,
387 Rockville (BRI), MD were housed at the Animal Research Facility of the George Washington
388 University Medical School, which is accredited by the American Association for Accreditation
389 of Laboratory Animal Care (AAALAC no. 000347) and has an Animal Welfare Assurance on
390 file with the National Institutes of Health, Office of Laboratory Animal Welfare, OLAW
391 assurance number A3205-01. All procedures employed were consistent with the Guide for the
392 Care and Use of Laboratory Animals. The Institutional Animal Care and Use Committee of the
393 George Washington University approved the protocol used for maintenance of mice and
394 recovery of schistosomes. Studies with BALB/c mice involving tail vein injection of schistosome

395 eggs and subsequent euthanasia using overdose of sodium pentobarbitone was approved by the
396 IACUC of the Biomedical Research Institute (BRI), protocol 18-04, AAALAC no. 000779 and
397 OLAW no. A3080-01.

398 **Schistosome eggs**

399 Mice were euthanized seven weeks after infection with *S. mansoni*, livers were removed at
400 necropsy, and schistosome eggs recovered from the livers, as described (77). The liver eggs
401 termed 'LE' were maintained in DMEM medium supplemented with 10% heat-inactivated fetal
402 bovine serum (FBS), 2% streptomycin/penicillin at 37°C under 5% CO_2 in air (76, 78).
403 Polymyxin B to (10 µg/ml) was added to the cultures twice daily to neutralize lipopolysaccharide
404 (LPS) (79). Soluble egg antigen (SEA) was prepared from these eggs, as described (23, 56). In
405 brief, the homogenate of eggs in 1×PBS containing protease inhibitor cocktail (Sigma) was
406 frozen and thawed twice, clarified by centrifugation at 13,000 rpm, 15 min, 4°C, the supernatant
407 passed through a 0.22-µm pore size membrane. Protein concentration of the supernatant (SEA)
408 was determined by the Bradford Protein Assay (80) and aliquots of the SEA stored at -80°C.

409 **Guide RNAs, Cas9, and single stranded DNA repair template**

410 Single guide RNA (sgRNA) was designed using the web-based tools at
411 http://bioinfogp.cnb.csic.es/tools/breakingcas/ (81) to predict cleavage sites for the *Streptococcus*
412 *pyogenes* Cas9 nuclease within the genome of *S. mansoni*. The sgRNA targeted exon 6 of the ω1
413 gene, Smp_193860, www.genedb.org, residues 3808-3827, adjacent to the protospacer adjacent
414 motif, AGG (Fig. 1a). This is a multi-copy gene with at least five copies of ω1 located in tandem
415 on chromosome 1 (12). To infer the gene structure of Smp_193860 in the *S. mansoni* V5
416 assembly more accurately, the omega-1 mRNA DQ013207.1 sequenced by Fitzsimmons *et al.*
417 (2005) (29) was used to predict the gene structure with the exonerate software, by aligning it to
418 the assembly using the exonerate options '--model coding2genome' and '--maxintron 1500'. The
419 Smp_193860 copy of ω1 includes nine exons interspersed with eight introns (6,196 nt) (Fig. 1a).

420 Synthetic gRNA (sgRNA), ω1-sgRNA was purchased from Thermo Fisher Scientific (Waltham,
421 MA). A double stranded DNA sequence complementary to the sgRNA was inserted into
422 lentiviral gene editing vector, pLV-U6g-EPCG (Sigma), which encodes Cas9 from *S. pyogenes*
423 driven by the eukaryotic (human) translation elongation factor 1 alpha 1 (tEF1) promoter and the
424 sgRNA driven by the human U6 promoter (Fig 1c). (The pLV-U6g-EPCG vector is tri-cistronic
425 and encodes the reporter genes encoding puroR and GFP, in addition to Cas9 (82).) This gene-
426 editing construct, targeting exon 6 of ω1 Smp_193860, was termed pLV-ω1X1. A single
427 stranded oligodeoxynucleotide (ssODN), which included homology arms of 50 nt each in length
428 at the 3' (position 3774-3824 nt) and 5' (3825-3874 nt) flanks and a small transgene (5'-
429 TAAGTGACTAGGTAACTGAGTAG-3', encoding stop codons (six) in all open-reading
430 frames) (Fig. 1b), was synthesized by Eurofin Genomics (KY, USA). An oligonucelotide primer
431 that included this sequence was employed in PCRs to investigate the presence of CRISPR/Cas9-
432 programmed insertion of the transgene (83) (Table s2).

433 **Transfection of schistosome eggs with a Cas9/guide RNA complex**

434 For the ribonucleoprotein (RNP) complex of the ω1-sgRNA and recombinant Cas 9 from
435 *Streptococcus pyogenes*, 3 μg of ω1-sgRNA and 3 μg of Cas9-NLS nuclease (Dharmacon,
436 Lafayette, CO) were mixed in 100 μl Opti-MEM (Sigma) to provide 1:1 ratio w/w RNP. The
437 mixture was incubated at room temperature for 10 min, pipetted into a 4 mm pre-chilled
438 electroporation cuvette containing ~10,000 LE in ~150 μl Opti-MEM, subjected to square wave
439 electroporation (one pulse of 125 volts, 20 milliseconds) (BTX ElectroSquarePorator, ECM830,
440 San Diego, CA). The electroporated eggs were incubated for 5 min at room temperature, and
441 maintained at 37°C, 5% CO_2 in air for 3, 5 and 7 days. To investigate whether homology-
442 directed repair (HDR) could catalyze the insertion of a donor repair template, 3 μg ssODN was
443 mixed with RNP and the LE before electroporation. In a second approach (above), the ssODN
444 was delivered to LE by electroporation at ~24 hours after the lentiviral transduction of the LE.
445 The eggs were collected 3, 5 and 7 days later and genomic DNA recovered from LE. The
446 negative controls included LE subjected to electroporation in the presence of only Opti-MEM,
447 only Cas 9, only sgRNA, and only ssODN.

448 **Transduction of schistosome eggs with lentiviral particles**

449 *Escherichia coli* Zymo 5α (Zymo Research) cells were transformed with lentiviral plasmid pLV-
450 ω1X1 and cultured in LB broth in 100 μg/ml ampicillin at 37°C, agitated at 225 rpm for ~18
451 hours, after which plasmid DNA was recovered (GenElute Plasmid purification kit, Invitrogen).
452 A lentiviral (LV) packaging kit (MISSION, Sigma-Aldrich) was used to prepare LV particles in
453 producer cells (human 293T cell line). In brief, 3.5×10^5 of 293T cells/well were seeded in a 6-
454 well tissue culture plate in DMEM supplemented with 10% heat- inactivated fetal bovine serum
455 (FBS), 2 mM L-glutamine, 1% penicillin/streptomycin and cultured at 37°C, 5% CO_2 for 18
456 hours. The producer cells were transfected using FUGENE HD (Promega) with pLV-ω1X1 and
457 LV packaging mix containing two additional plasmids; one plasmid that expressed HIV
458 structural and packaging genes and another that expressed the pseudotyping envelope protein
459 Vesicular Stomatitis Virus Glycoprotein (VSVG). Subsequently, the transfection mixture (50 μl;
460 500 ng plasmid DNA, 4.6 μl packaging mix, 2.7 μl of FUGENE HD in Opti-MEM) was
461 dispensed drop wise into each well on the plate. Sixteen hours later, the media were removed
462 from the transfected cells, replaced with pre-warmed complete DMEM, and cells cultured for 24
463 hours. The supernatant, containing VSVG-pseudotyped LV particles was filtered through 22 μm
464 pore size membranes (45), and stored at 4°C. Additional pre-warmed complete DMEM was
465 added to the well, for culture for a further 24 hours. The supernatant was collected as above,
466 combined with the first supernatant and concentrated (Lenti-X concentrator, Takara Bio,
467 Mountain View, CA). Virion titer was estimated by two methods; first, by use of Lenti-X-
468 GoStix (Takara Bio) to establish the presence of functional virions at $>10^5$ infectious units
469 (IFU)/ml, and second, by reverse transcriptase assay (45, 84) to quantify levels of active virions.
470 Virions with counts of $\sim 4\times10^6$ count per minute (cpm)/ml were aliquoted and stored at -80°C.

471 To transduce LE with LV, ~10,000 eggs were incubated for 24 hours in complete DMEM
472 containing 500 μl of $\sim 4\times10^6$ cpm/ml VSVG-LV virions. Thereafter, the LE were washed three
473 times in 1×PBS and transfected with ssODN by square wave electroporation or further steps. LV
474 virions heat-inactivated by incubation at 70°C for two hours (45) with subsequent transfection
475 with the ssODN, transfection with ssODN in the absence of virions or Opti-MEM only served as
476 negative controls.

477 **PCR amplification of diagnostic transgene to detect knock-in into exon 6 of ω1**

478 For each DNA sample, four separate PCR assays using four distinct primer pairs (Table s2) were
479 carried out. The first ω1 primer pair, to amplify locations 3751-4740 nt of Smp_193860, was
480 employed as positive control for the presence of genomic DNA with the Smp_193860 copy of
481 *ω1*. The other primer pairs shared one forward primer complementary to the knock-in 24 nt
482 transgene with three reverse primers, Sm ω1-R1, -R2 and -R3 at positions 3966-3984, 4066-4085
483 and 4102-4121 nt, respectively, binding to three sites downstream of the ω1 predicted DSB site
484 (Fig. 2a; Table s2) (83). The PCR mix included 10 µl Green GoTaq DNA polymerase mix
485 (Promega) with 200 nM of each primer and 10 ng genomic DNA. Thermal cycling conditions
486 involved denaturation at 95°C, 3 min followed by 30 cycles of 94°C, 30 seconds, 60°C, 30
487 seconds and 72°C, 30 seconds and a final extension at 72°C for 5 minutes. Following agarose gel
488 electrophoresis (1.2% agarose/TAE), amplicons of the expected sizes were recovered from gels
489 and ligated into pCR4-TOPO (Thermo Fisher). *E. coli* Zymo 5α competent cells were
490 transformed with the ligation products, several colonies of each transformant were grown under
491 ampicillin selection, plasmid DNA purified, and insert sequenced to confirm the presence and
492 knock-in of the transgene (Fig. 1c).

493 **Illumina sequencing**

494 Pooled LE DNA samples from six independent KI experiments of pLV-ω1X1 with ssODN were
495 used as the template to amplify the on-target DNA fragment using MiSeq primers (Fig. 2a) with
496 High Fidelity *Taq* DNA polymerase (Thermo Fisher). PCR reactions were set up with 10 ng LE
497 DNA samples from the KI experiment in 25 µl reaction mix using the HiFidelity Taq DNA
498 polymerase (Thermo Fisher) following the PCR program 94ºC for 3 minutes of denaturation
499 followed by 30 cycles of 94ºC for 30 seconds, 60ºC or 54ºC for 30 seconds, 72ºC for 45 seconds
500 and final extension at 72ºC for 2 minutes. The expected size of the amplicon flanking predicted
501 DSB was 205 bp. Amplicons of this size were purified using the Agencourt AMPure XP system
502 (Beckman Coulter). Amplicons generated from four different PCR reactions from each sample
503 were pooled, and 100 ng of amplicons from each sample was used to construct the uniquely
504 indexed paired-end read libraries using the QIAseq 1-step Amplicon Library Kit (Qiagen) and
505 GeneRead Adapter I set A 12-plex (Qiagen). These libraries were pooled, and the library pool
506 was quantified using the QIAseq Library Quant System (Qiagen).

507 Samples (Table s3) were multiplexed (10 samples) and each run on four MiSeq lanes. After
508 sequencing, the fastq files for each particular sample were merged. Samples 1-6, 8 and 10 were
509 prepared using an annealing temperature of 54ºC. Samples 7 and 9 were prepared using an
510 annealing temperature of 60ºC, and included an extra 10 bp at the start of the MiSeq sequences,
511 'GTTTTAGGTC', present upstream of the 5' primer in the genomic DNA. We trimmed this
512 sequence from the reads using cutadapt v1.13 (85). To detect HDR events, CRISPResso v1.0.9
513 (48, 86) was employed using a window size of 500 bp (-w 500) with the reference amplicon
514 according to gene *Smp_193860* in the *S. mansoni* V7 assembly, and with the --
515 exclude_bp_from_left 25 and --exclude_bp_from_right 25 options in order to disregard the (24
516 bp) primer regions on each end of the amplicon when indels are being quantified. A window size
517 of 500 nt was employed to include the entire amplicon. In order to search for HDR events,
518 CRISPResso checked for HDR events (using –e and –d options) in treatment groups including
519 controls. To infer frameshifts using CRISPResso the –c option was used, giving CRISPResso the

520 coding sequence from positions 42-179 of the amplicon. To confirm the insertions of the knock-
521 in sequences reported by CRISPResso (column L in Table s3), we took all insertions of 20-28 bp
522 reported by CRISPResso, and calculated their percent identity to the expected knock-in sequence
523 using ggsearch v36.3.5e in the fasta package (87), and an insertion was considered confirmed if
524 it shared ≥75% identity to the expected donor knock-in sequence.

525 **Copy number estimation for *ω1***

526 A quantitative PCR to estimate the relative copy number of ω1 was performed using Kapa qPCR
527 mastermix SYBRfast (KK4602) on 1 ng of gDNA templates isolated from control and test
528 samples, in 20 µl volumes. Primer pair OMGgRNA1F and OMGgRNA1R was used to amplify
529 the ω1 gRNA target region and SmGAPDH (Smp_056970) as a reference single-copy gene
530 (primers shown in Table s2). The PCR efficiencies for primer pairs were estimated by titration
531 analysis to be 100% ±5 (88) and qPCRs were performed in triplicate in 96-well plates, with a
532 denaturation step at 95°C of 3 min followed by 40 cycles of 30 sec at 95°C and 30 sec at 55°C,
533 in thermal cycler fitted with a real time detector (StepOnePlus, Applied Biosystem). The relative
534 quantification assay $2^{-\Delta\Delta Ct}$ method (89) was used to ascertain the relative copy number of *ω1*.
535 Relative copy number of *ω1* in the CRISPR/Cas9 treated groups reflects the fold change of *ω1*
536 copy number normalized to the reference gene (Sm GAPDH) and relative to the untreated
537 control group (calibrator sample with relative *ω1* copy number = 1) (49).

538 **Gene expression for *ω1* mRNA**

539 Total RNAs from schistosome eggs were extracted using the RNAzol RT reagent (Molecular
540 Research Center, Inc), which eliminates contaminating DNA (90), and concentration and purity
541 determined using a spectrophotometer ($OD_{260/280}$ ~2.0). Reverse transcription (RT) of the RNA
542 (500 ng) was performed using iScript Reverse Transcript (Bio-Rad), after which first strand
543 cDNA was employed as template for qPCRs using SsoAdvanced Universal SYBR Green
544 Supermix (Bio-Rad) performed in triplicates in an iQ5 real time thermal cycler (Bio-Rad). RT-
545 qPCR reaction mixtures included 2 µl first strand cDNA, 5 µl SsoAdvanced Universal SYBR
546 Green Supermix, and 300 nM schistosome gene specific primers. Table s2 provides details of the
547 oligonucleotide primers. Thermal cycling included denaturation at 95°C for 30 sec, 40
548 amplification cycles each consisting of denaturation at 95°C for 15 sec and annealing/extension
549 at 60°C for 30 sec, and a final melting curve. The output was analyzed using the iQ5 software.
550 Relative expression was calculated using the $2^{-\Delta\Delta Ct}$ method and normalized to schistosome
551 GAPDH expression (89); data are presented as transcript levels (three replicates) compared to
552 the WT (100%) LE, and fold change reported as mean relative expression ± SD.

553 **Nuclease activity of ω1**

554 A stock solution of yeast RNA (Omega Bio-tek, Norcross, GA) was prepared at 1.0 µg/µl, 50
555 mM Tris-HCl, 50 mM NaCl, pH 7.0. Yeast RNA (200 ng) was incubated with 2 µg SEA from
556 control and experimental groups individually at 37°C for 60 min. (SEA investigated here, named
557 Δω1-SEA, was extracted from LE transduced with pLV- ω1X1 virions and ssODN, pooled from
558 six biological replicates.) RNase A, an endoribonuclease from bovine pancreas (Thermo Fisher)
559 served as a positive control enzyme whereas yeast RNA in reaction buffer only served as the

560 negative control. The RNase activity of ω1 in wild type SEA or Δω1-SEA was analyzed by
561 visualizing and quantifying the substrate that remained following enzymolysis by agarose gel
562 electrophoresis and staining with ethidium bromide. The yeast RNA digestion by control SEAs
563 or Δω1-SEA were set up in triplicates, with quantity of residual RNA determined by
564 densitometry (50).

565 **Macrophage polarization by WT or Δω1-SEA and T-cell activation *in vitro***

566 Human monocytic THP-1 cells were maintained in Roswell Park Memorial Institute medium
567 (RPMI) 1640 with L-glutamine, HEPES (Thermo Fisher Scientific) containing 10% (v/v) FBS
568 with 4 mM glutamine, 25 mM HEPES, 2.5 g/L D-glucose at 37°C in 5% CO_2 in air. THP-1 cells
569 were non-adherent cells. In a 6-well plate, THP-1 monocytes (3×10^5 cells in each well) were
570 differentiated into macrophages (Mϕ) by incubation in 150 nM phorbol 12-myristate 13-acetate
571 (PMA) (Sigma) for 48 hours (91). Mϕ were exposed to SEA (50 ng/ml) or Δω1-SEA (50 ng/ml)
572 (from LE transduced with pLV-ω1X1 virions and ssODN) for 48 hours. To investigate
573 macrophage and T cell interactions, Mϕ cells were pulsed with 50 ng/ml SEA or Δω1-SEA and
574 thereafter co-cultured in direct contact with Jurkat (human $CD4^+$ T) cells. Nine $\times10^5$ Jurkat were
575 added to Mϕ with direct contactand were co-cultured for an additional 72 hours. Cell-free
576 supernatants from the co-cultures were collected to quantify secretion of T helper cell cytokines
577 including IL-4, IL-5, IL-13, IL-10, TNF-α, IL-6, IL-2 and IFN-γ by enzyme linked
578 immunosorbent assay (ELISA) (Qiagen) (92). The assay included positive controls for each
579 analyte, which were provided in the ELISA kit (Qiagen). Three biological replicates were
580 undertaken.

581 **Schistosome egg-induced primary pulmonary granulomas**

582 For induction of circumoval, egg-induced granulomas in the lungs of mice, 8 week old female
583 (25) BALB/c mice were injected with 3,000 WT eggs or Δω1-eggs (from experiment pLV-ω1X1
584 with ssODN) or 1×PBS as negative control by tail vein, as described (58). The mice (6-9
585 mice/group) were euthanized 10 days later. For histopathological assessment of granuloma
586 formation, the left lung was removed at necropsy and fixed in 10% formalin in pH 7.4 buffered
587 saline for 24 hours, after which it was dehydrated in 70% ethanol, and clarified in xylene. The
588 fixed lung tissue was embedded in paraffin and sectioned at 4-µm-thickness by microtome (58).
589 Thin sections of the left lung lobe were mounted on glass slides and fixed at 58-60°C.
590 Subsequently, rehydrated sections were stained with hematoxylin-eosin (H&E) for evaluation of
591 inflammatory infiltrates and cellularity of granulomas. The longest (R) and shortest (r) diameters
592 of each granuloma containing a single egg were measured with an ocular micrometer, and the
593 volume of the granuloma calculated assuming a prolate spheroidal shape, using $4/3\ \pi\ Rr^2$ (25).
594 All granulomas in all slides from the left lung of the mice, 15 slides per treatment group, were
595 measured; in total, >100 granulomas from each treatment group. Digital images were captured
596 using a 2D glass slide digital scanner (Aperio Slide Scanner, Leica Biosystems, Vista, CA) and
597 examined at high magnification using the Aperio ImageScope (Leica) software (57, 93).

598 **Statistics**

599 Means for experimental groups were compared to controls by one-way ANOVA and, where
600 appropriate, by two-tailed Student's *t*-test and Welch's unequal variances *t*-test (GraphPad
601 Prism, La Jolla, CA). Values for p of ≤ 0.05 were considered to be statistically significant.

602 **Acknowledgements**

603 We thank Dragana Jankovic, Alan Sher, Thomas Wynn, Michael Bukrinsky, Larisa Dubrovsky,
604 Arnon Jurberg, Meredith Brindley, Robert Thompson and Thiago De Almeida Pereira for advice
605 and technical assistance. Schistosome-infected mice and snails were provided by the NIAID
606 Schistosomiasis Resource Center of the Biomedical Research Institute, Rockville, Maryland
607 through NIH-NIAID Contract HHSN272201000005I for distribution through BEI Resources.
608 We acknowledge the Thailand Research Fund through Senior Research Scholar Grant (RR, W.
609 Maleewong) and the Royal Golden Jubilee Ph.D. program numbers PHD/0011/2555 (AC, S.
610 Pinlaor), PHD/0047/2556 (PP, Nitat Sookrung), PHD/0053/2556 (RR, W. Maleewong). These
611 studies were supported by Wellcome Trust Strategic Award number 107475/Z/15/Z (KFH,
612 principal investigator), Wellcome Trust grant WT 098051 award (MB), R21AI109532 (GR, PJB)
613 award from NIAID, National Institutes of Health, and, in part, by generous support from
614 MaxMind Inc./TJ Mather (PJB).

615

616 **References**

617 1. Gryseels B, Polman K, Clerinx J, Kestens L. Human schistosomiasis. Lancet.
618 2006;368(9541):1106-18.
619 2. Hotez PJ, Brindley PJ, Bethony JM, King CH, Pearce EJ, Jacobson J. Helminth
620 infections: the great neglected tropical diseases. J Clin Invest. 2008;118(4):1311-21.
621 3. Hotez PJ, Alvarado M, Basanez MG, Bolliger I, Bourne R, Boussinesq M, et al. The
622 global burden of disease study 2010: interpretation and implications for the neglected tropical
623 diseases. PLoS Negl Trop Dis. 2014;8(7):e2865.
624 4. Colley DG, Bustinduy AL, Secor WE, King CH. Human schistosomiasis. Lancet.
625 2014;383(9936):2253-64.
626 5. Berriman M, Haas BJ, LoVerde PT, Wilson RA, Dillon GP, Cerqueira GC, et al. The
627 genome of the blood fluke Schistosoma mansoni. Nature. 2009;460(7253):352-8.
628 6. Schistosoma japonicum Genome S, Functional Analysis C. The Schistosoma japonicum
629 genome reveals features of host-parasite interplay. Nature. 2009;460(7253):345-51.
630 7. Young ND, Jex AR, Li B, Liu S, Yang L, Xiong Z, et al. Whole-genome sequence of
631 Schistosoma haematobium. Nat Genet. 2012;44(2):221-5.
632 8. Lepesant JM, Grunau C, Cosseau C. Towards an understanding of the epigenetics of
633 schistosomes: a comparative epigenomic study. Mem Inst Oswaldo Cruz. 2011;106(7):823-30.
634 9. Geyer KK, Rodriguez Lopez CM, Chalmers IW, Munshi SE, Truscott M, Heald J, et al.
635 Cytosine methylation regulates oviposition in the pathogenic blood fluke Schistosoma mansoni.
636 Nat Commun. 2011;2:424.
637 10. Vanderstraete M, Gouignard N, Cailliau K, Morel M, Hahnel S, Leutner S, et al. Venus
638 kinase receptors control reproduction in the platyhelminth parasite Schistosoma mansoni. PLoS
639 Pathog. 2014;10(5):e1004138.
640 11. Rinaldi G, Eckert SE, Tsai IJ, Suttiprapa S, Kines KJ, Tort JF, et al. Germline
641 transgenesis and insertional mutagenesis in Schistosoma mansoni mediated by murine leukemia
642 virus. PLoS Pathog. 2012;8(7):e1002820.
643 12. Protasio AV, Tsai IJ, Babbage A, Nichol S, Hunt M, Aslett MA, et al. A systematically
644 improved high quality genome and transcriptome of the human blood fluke Schistosoma
645 mansoni. PLoS Negl Trop Dis. 2012;6(1):e1455.
646 13. Valentim CL, Cioli D, Chevalier FD, Cao X, Taylor AB, Holloway SP, et al. Genetic and
647 molecular basis of drug resistance and species-specific drug action in schistosome parasites.
648 Science. 2013;342(6164):1385-9.
649 14. Wang B, Collins JJ, 3rd, Newmark PA. Functional genomic characterization of neoblast-
650 like stem cells in larval Schistosoma mansoni. Elife. 2013;2:e00768.
651 15. Collins JJ, 3rd, Wang B, Lambrus BG, Tharp ME, Iyer H, Newmark PA. Adult somatic
652 stem cells in the human parasite Schistosoma mansoni. Nature. 2013;494(7438):476-9.
653 16. Hagen J, Young ND, Every AL, Pagel CN, Schnoeller C, Scheerlinck JP, et al. Omega-1
654 knockdown in Schistosoma mansoni eggs by lentivirus transduction reduces granuloma size in
655 vivo. Nat Commun. 2014;5:5375.
656 17. Hoffmann KF, Brindley PJ, Berriman M. Medicine. Halting harmful helminths. Science.
657 2014;346(6206):168-9.
658 18. Pearce EJ, MacDonald AS. The immunobiology of schistosomiasis. Nat Rev Immunol.
659 2002;2(7):499-511.

660 19. Steinfelder S, Andersen JF, Cannons JL, Feng CG, Joshi M, Dwyer D, et al. The major
661 component in schistosome eggs responsible for conditioning dendritic cells for Th2 polarization
662 is a T2 ribonuclease (omega-1). J Exp Med. 2009;206(8):1681-90.
663 20. Everts B, Perona-Wright G, Smits HH, Hokke CH, van der Ham AJ, Fitzsimmons CM, et
664 al. Omega-1, a glycoprotein secreted by Schistosoma mansoni eggs, drives Th2 responses. J Exp
665 Med. 2009;206(8):1673-80.
666 21. Pearce EJ, C MK, Sun J, J JT, McKee AS, Cervi L. Th2 response polarization during
667 infection with the helminth parasite Schistosoma mansoni. Immunol Rev. 2004;201:117-26.
668 22. Everts B, Hussaarts L, Driessen NN, Meevissen MH, Schramm G, van der Ham AJ, et al.
669 Schistosome-derived omega-1 drives Th2 polarization by suppressing protein synthesis
670 following internalization by the mannose receptor. J Exp Med. 2012;209(10):1753-67, S1.
671 23. Dunne DW, Jones FM, Doenhoff MJ. The purification, characterization, serological
672 activity and hepatotoxic properties of two cationic glycoproteins (alpha 1 and omega 1) from
673 Schistosoma mansoni eggs. Parasitology. 1991;103 Pt 2:225-36.
674 24. Curwen RS, Ashton PD, Johnston DA, Wilson RA. The Schistosoma mansoni soluble
675 proteome: a comparison across four life-cycle stages. Mol Biochem Parasitol. 2004;138(1):57-
676 66.
677 25. Ashton PD, Harrop R, Shah B, Wilson RA. The schistosome egg: development and
678 secretions. Parasitology. 2001;122(Pt 3):329-38.
679 26. Cass CL, Johnson JR, Califf LL, Xu T, Hernandez HJ, Stadecker MJ, et al. Proteomic
680 analysis of Schistosoma mansoni egg secretions. Mol Biochem Parasitol. 2007;155(2):84-93.
681 27. Mathieson W, Wilson RA. A comparative proteomic study of the undeveloped and
682 developed Schistosoma mansoni egg and its contents: the miracidium, hatch fluid and secretions.
683 Int J Parasitol. 2010;40(5):617-28.
684 28. Wilbers RH, Westerhof LB, van Noort K, Obieglo K, Driessen NN, Everts B, et al.
685 Production and glyco-engineering of immunomodulatory helminth glycoproteins in plants. Sci
686 Rep. 2017;7:45910.
687 29. Fitzsimmons CM, Schramm G, Jones FM, Chalmers IW, Hoffmann KF, Grevelding CG,
688 et al. Molecular characterization of omega-1: a hepatotoxic ribonuclease from Schistosoma
689 mansoni eggs. Mol Biochem Parasitol. 2005;144(1):123-7.
690 30. Ferguson BJ, Newland SA, Gibbs SE, Tourlomousis P, Fernandes dos Santos P, Patel
691 MN, et al. The Schistosoma mansoni T2 ribonuclease omega-1 modulates inflammasome-
692 dependent IL-1beta secretion in macrophages. Int J Parasitol. 2015;45(13):809-13.
693 31. Wynn TA, Thompson RW, Cheever AW, Mentink-Kane MM. Immunopathogenesis of
694 schistosomiasis. Immunol Rev. 2004;201:156-67.
695 32. Jinek M, Chylinski K, Fonfara I, Hauer M, Doudna JA, Charpentier E. A programmable
696 dual-RNA-guided DNA endonuclease in adaptive bacterial immunity. Science.
697 2012;337(6096):816-21.
698 33. Hsu PD, Lander ES, Zhang F. Development and applications of CRISPR-Cas9 for
699 genome engineering. Cell. 2014;157(6):1262-78.
700 34. Murare HM, Dunne DW, Bain J, Doenhoff MJ. Schistosoma mansoni: control of
701 hepatotoxicity and egg excretion by immune serum in infected immunosuppressed mice is
702 schistosome species-specific, but not S. mansoni strain-specific. Exp Parasitol. 1992;75(3):329-
703 39.
704 35. Luhtala N, Parker R. T2 Family ribonucleases: ancient enzymes with diverse roles.
705 Trends Biochem Sci. 2010;35(5):253-9.

706 36. M LZZYB. A web portal for gene expression across all life stages of Schistosoma
707 mansoni. bioRxiv. 2018.
708 37. Lee AH, Symington LS, Fidock DA. DNA repair mechanisms and their biological roles
709 in the malaria parasite Plasmodium falciparum. Microbiol Mol Biol Rev. 2014;78(3):469-86.
710 38. Deriano L, Roth DB. Modernizing the nonhomologous end-joining repertoire: alternative
711 and classical NHEJ share the stage. Annu Rev Genet. 2013;47:433-55.
712 39. Pardo B, Gomez-Gonzalez B, Aguilera A. DNA repair in mammalian cells: DNA double-
713 strand break repair: how to fix a broken relationship. Cell Mol Life Sci. 2009;66(6):1039-56.
714 40. Consortium IHG. Comparative genomics of the major parasitic worms. bioRxiv.
715 2017;https://www.biorxiv.org/content/early/2017/12/20/236539
716 41. Lok JB, Shao H, Massey HC, Li X. Transgenesis in Strongyloides and related parasitic
717 nematodes: historical perspectives, current functional genomic applications and progress towards
718 gene disruption and editing. Parasitology. 2017;144(3):327-42.
719 42. Gang SS, Castelletto ML, Bryant AS, Yang E, Mancuso N, Lopez JB, et al. Targeted
720 mutagenesis in a human-parasitic nematode. PLoS Pathog. 2017;13(10):e1006675.
721 43. Chen F, Pruett-Miller SM, Davis GD. Gene editing using ssODNs with engineered
722 endonucleases. Methods Mol Biol. 2015;1239:251-65.
723 44. Duvoisin R, Ayuk MA, Rinaldi G, Suttiprapa S, Mann VH, Lee CM, et al. Human U6
724 promoter drives stronger shRNA activity than its schistosome orthologue in Schistosoma
725 mansoni and human fibrosarcoma cells. Transgenic Res. 2012;21(3):511-21.
726 45. Suttiprapa S, Rinaldi G, Tsai IJ, Mann VH, Dubrovsky L, Yan HB, et al. HIV-1
727 Integrates Widely throughout the Genome of the Human Blood Fluke Schistosoma mansoni.
728 PLoS Pathog. 2016;12(10):e1005931.
729 46. Shah AN, Davey CF, Whitebirch AC, Miller AC, Moens CB. Rapid reverse genetic
730 screening using CRISPR in zebrafish. Nat Methods. 2015;12(6):535-40.
731 47. Yu C, Zhang Y, Yao S, Wei Y. A PCR based protocol for detecting indel mutations
732 induced by TALENs and CRISPR/Cas9 in zebrafish. PLoS One. 2014;9(6):e98282.
733 48. Pinello L, Canver MC, Hoban MD, Orkin SH, Kohn DB, Bauer DE, et al. Analyzing
734 CRISPR genome-editing experiments with CRISPResso. Nat Biotechnol. 2016;34(7):695-7.
735 49. Suttiprapa S, Rinaldi G, Brindley PJ. Prototypic chromatin insulator cHS4 protects
736 retroviral transgene from silencing in Schistosoma mansoni. Transgenic Res. 2012;21(3):555-66.
737 50. Ke XD, Shen S, Song LJ, Yu CX, Kikuchi M, Hirayama K, et al. Characterization of
738 Schistosoma japonicum CP1412 protein as a novel member of the ribonuclease T2 molecule
739 family with immune regulatory function. Parasit Vectors. 2017;10(1):89.
740 51. Zaccone P, Burton OT, Gibbs SE, Miller N, Jones FM, Schramm G, et al. The S. mansoni
741 glycoprotein omega-1 induces Foxp3 expression in NOD mouse CD4(+) T cells. European
742 journal of immunology. 2011;41(9):2709-18.
743 52. Ritter M, Gross O, Kays S, Ruland J, Nimmerjahn F, Saijo S, et al. Schistosoma mansoni
744 triggers Dectin-2, which activates the Nlrp3 inflammasome and alters adaptive immune
745 responses. Proceedings of the National Academy of Sciences of the United States of America.
746 2010;107(47):20459-64.
747 53. Qin Z. The use of THP-1 cells as a model for mimicking the function and regulation of
748 monocytes and macrophages in the vasculature. Atherosclerosis. 2012;221(1):2-11.
749 54. Fuentes L, Hernandez M, Fernandez-Aviles FJ, Crespo MS, Nieto ML. Cooperation
750 between secretory phospholipase A2 and TNF-receptor superfamily signaling: implications for
751 the inflammatory response in atherogenesis. Circulation research. 2002;91(8):681-8.

752 55. Doenhoff MJ, Hassounah O, Murare H, Bain J, Lucas S. The schistosome egg
753 granuloma: immunopathology in the cause of host protection or parasite survival? Trans R Soc
754 Trop Med Hyg. 1986;80(4):503-14.
755 56. Boros DL, Warren KS. Delayed hypersensitivity-type granuloma formation and dermal
756 reaction induced and elicited by a soluble factor isolated from Schistosoma mansoni eggs. J Exp
757 Med. 1970;132(3):488-507.
758 57. Eltoum IA, Wynn TA, Poindexter RW, Finkelman FD, Lewis FA, Sher A, et al.
759 Suppressive effect of interleukin-4 neutralization differs for granulomas around Schistosoma
760 mansoni eggs injected into mice compared with those around eggs laid in infected mice. Infect
761 Immun. 1995;63(7):2532-6.
762 58. Wynn TA, Eltoum I, Cheever AW, Lewis FA, Gause WC, Sher A. Analysis of cytokine
763 mRNA expression during primary granuloma formation induced by eggs of Schistosoma
764 mansoni. J Immunol. 1993;151(3):1430-40.
765 59. Lieber MR. The mechanism of double-strand DNA break repair by the nonhomologous
766 DNA end-joining pathway. Annu Rev Biochem. 2010;79:181-211.
767 60. Paquet D, Kwart D, Chen A, Sproul A, Jacob S, Teo S, et al. Efficient introduction of
768 specific homozygous and heterozygous mutations using CRISPR/Cas9. Nature.
769 2016;533(7601):125-9.
770 61. Zhang WW, Matlashewski G. CRISPR-Cas9-Mediated Genome Editing in Leishmania
771 donovani. MBio. 2015;6(4):e00861.
772 62. Yoshimi K, Kunihiro Y, Kaneko T, Nagahora H, Voigt B, Mashimo T. ssODN-mediated
773 knock-in with CRISPR-Cas for large genomic regions in zygotes. Nature communications.
774 2016;7:10431.
775 63. Kosicki M, Rajan SS, Lorenzetti FC, Wandall HH, Narimatsu Y, Metzakopian E, et al.
776 Dynamics of Indel Profiles Induced by Various CRISPR/Cas9 Delivery Methods. Prog Mol Biol
777 Transl Sci. 2017;152:49-67.
778 64. Holmgaard A, Askou AL, Benckendorff JNE, Thomsen EA, Cai Y, Bek T, et al. In Vivo
779 Knockout of the Vegfa Gene by Lentiviral Delivery of CRISPR/Cas9 in Mouse Retinal Pigment
780 Epithelium Cells. Mol Ther Nucleic Acids. 2017;9:89-99.
781 65. Yu Z, Chen Q, Chen W, Zhang X, Mei F, Zhang P, et al. Multigene editing via
782 CRISPR/Cas9 guided by a single-sgRNA seed in Arabidopsis. J Integr Plant Biol.
783 2018;60(5):376-81.
784 66. Luo JJ, Bian WP, Liu Y, Huang HY, Yin Q, Yang XJ, et al. CRISPR/Cas9-based genome
785 engineering of zebrafish using a seamless integration strategy. FASEB J. 2018:fj201800077RR.
786 67. Shalem O, Sanjana NE, Zhang F. High-throughput functional genomics using CRISPR-
787 Cas9. Nat Rev Genet. 2015;16(5):299-311.
788 68. Jurberg AD, Goncalves T, Costa TA, de Mattos AC, Pascarelli BM, de Manso PP, et al.
789 The embryonic development of Schistosoma mansoni eggs: proposal for a new staging system.
790 Dev Genes Evol. 2009;219(5):219-34.
791 69. Neill PJ, Smith JH, Doughty BL, Kemp M. The ultrastructure of the Schistosoma
792 mansoni egg. Am J Trop Med Hyg. 1988;39(1):52-65.
793 70. Mann VH, Suttiprapa S, Rinaldi G, Brindley PJ. Establishing transgenic schistosomes.
794 PLoS Negl Trop Dis. 2011;5(8):e1230.
795 71. Heyer WD, Ehmsen KT, Liu J. Regulation of homologous recombination in eukaryotes.
796 Annu Rev Genet. 2010;44:113-39.

797 72. Schramm G, Hamilton JV, Balog CI, Wuhrer M, Gronow A, Beckmann S, et al.
798 Molecular characterisation of kappa-5, a major antigenic glycoprotein from Schistosoma
799 mansoni eggs. Mol Biochem Parasitol. 2009;166(1):4-14.
800 73. Lu Z, ; Zhang, Y.; Berriman, M. A web portal for gene expression across all life stages of
801 Schistosoma mansoni. bioRxiv. 2018.
802 74. MacDonald AS, Araujo MI, Pearce EJ. Immunology of parasitic helminth infections.
803 Infect Immun. 2002;70(2):427-33.
804 75. Kaisar MMM, Ritter M, Del Fresno C, Jonasdottir HS, van der Ham AJ, Pelgrom LR, et
805 al. Dectin-1/2-induced autocrine PGE2 signaling licenses dendritic cells to prime Th2 responses.
806 PLoS Biol. 2018;16(4):e2005504.
807 76. Mann VH, Suttiprapa S, Skinner DE, Brindley PJ, Rinaldi G. Pseudotyped murine
808 leukemia virus for schistosome transgenesis: approaches, methods and perspectives. Transgenic
809 Res. 2014;23(3):539-56.
810 77. Dalton JP, Day SR, Drew AC, Brindley PJ. A method for the isolation of schistosome
811 eggs and miracidia free of contaminating host tissues. Parasitology. 1997;115 (Pt 1):29-32.
812 78. Mann VH, Morales ME, Rinaldi G, Brindley PJ. Culture for genetic manipulation of
813 developmental stages of Schistosoma mansoni. Parasitology. 2010;137(3):451-62.
814 79. Cardoso LS, Araujo MI, Goes AM, Pacifico LG, Oliveira RR, Oliveira SC. Polymyxin B
815 as inhibitor of LPS contamination of Schistosoma mansoni recombinant proteins in human
816 cytokine analysis. Microb Cell Fact. 2007;6:1.
817 80. Bradford MM. A rapid and sensitive method for the quantitation of microgram quantities
818 of protein utilizing the principle of protein-dye binding. Anal Biochem. 1976;72:248-54.
819 81. Oliveros JC, Franch M, Tabas-Madrid D, San-Leon D, Montoliu L, Cubas P, et al.
820 Breaking-Cas-interactive design of guide RNAs for CRISPR-Cas experiments for ENSEMBL
821 genomes. Nucleic Acids Res. 2016;44(W1):W267-71.
822 82. Minskaia E, Nicholson J, Ryan MD. Optimisation of the foot-and-mouth disease virus 2A
823 co-expression system for biomedical applications. BMC Biotechnol. 2013;13:67.
824 83. Lok JB, Shao H, Massey HC, Li X. Transgenesis in Strongyloides and related parasitic
825 nematodes: historical perspectives, current functional genomic applications and progress towards
826 gene disruption and editing. Parasitology. 2016:1-16.
827 84. Marozsan AJ, Fraundorf E, Abraha A, Baird H, Moore D, Troyer R, et al. Relationships
828 between infectious titer, capsid protein levels, and reverse transcriptase activities of diverse
829 human immunodeficiency virus type 1 isolates. J Virol. 2004;78(20):11130-41.
830 85. Martin M. Cutadapt removes adapter sequences from high-throughput sequencing reads.
831 EMBnetjournal North America.
832 2011;http://journal.embnet.org/index.php/embnetjournal/article/view/200/458.
833 86. Canver MC, Haeussler M, Bauer DE, Orkin SH, Sanjana NE, Shalem O, et al. Integrated
834 design, execution, and analysis of arrayed and pooled CRISPR genome-editing experiments. Nat
835 Protoc. 2018;13(5):946-86.
836 87. Pearson WR, Lipman DJ. Improved tools for biological sequence comparison. Proc Natl
837 Acad Sci U S A. 1988;85(8):2444-8.
838 88. Ginzinger DG. Gene quantification using real-time quantitative PCR: an emerging
839 technology hits the mainstream. Exp Hematol. 2002;30(6):503-12.
840 89. Livak KJ, Schmittgen TD. Analysis of relative gene expression data using real-time
841 quantitative PCR and the 2(-Delta Delta C(T)) Method. Methods. 2001;25(4):402-8.

842 90. Chomczynski P. A reagent for the single-step simultaneous isolation of RNA, DNA and
843 proteins from cell and tissue samples. Biotechniques. 1993;15(3):532-4, 6-7.
844 91. Genin M, Clement F, Fattaccioli A, Raes M, Michiels C. M1 and M2 macrophages
845 derived from THP-1 cells differentially modulate the response of cancer cells to etoposide. BMC
846 Cancer. 2015;15:577.
847 92. Schmid MC, Varner JA. Myeloid cells in the tumor microenvironment: modulation of
848 tumor angiogenesis and tumor inflammation. Journal of oncology. 2010;2010:201026.
849 93. Cheever AW, Finkelman FD, Caspar P, Heiny S, Macedonia JG, Sher A. Treatment with
850 anti-IL-2 antibodies reduces hepatic pathology and eosinophilia in Schistosoma mansoni-
851 infected mice while selectively inhibiting T cell IL-5 production. Journal of immunology.
852 1992;148(10):3244-8.
853 94. Crooks GE, Hon G, Chandonia JM, Brenner SE. WebLogo: a sequence logo generator.
854 Genome Res. 2004;14(6):1188-90.
855 95. Gieseck RL, 3rd, Wilson MS, Wynn TA. Type 2 immunity in tissue repair and fibrosis.
856 Nat Rev Immunol. 2018;18(1):62-76.
857 96. Wynn TA. Type 2 cytokines: mechanisms and therapeutic strategies. Nat Rev Immunol.
858 2015;15(5):271-82.
859 97. Larkin MA, Blackshields G, Brown NP, Chenna R, McGettigan PA, McWilliam H, et al.
860 Clustal W and Clustal X version 2.0. Bioinformatics. 2007;23(21):2947-8.
861
862

863 **Figure legends**

864 **Figure 1. Genomic structure of the locus encoding omega-1 (ω1) in the genome of**
865 ***Schistosoma mansoni,* guide RNA and CRISPR/Cas9 encoding construct.** Gene model of **ω**1
866 (*Smp_193860*), showing the position of its nine exons, eight introns and UTRs 6,196 bp on
867 chromosome 1 (**a**). Nucleotide sequence in exon 6 indicating location and sequence of gRNA
868 target site, predicted double stranded break (DSB) (arrow), protospacer adjacent motif (PAM)
869 (AGG, blue box), and 124-nucleotide sequence of the single stranded DNA donor template
870 provided for DSB repair by homologous recombination. Homology arms of 50 nt span a central
871 24 nt of six-stop-codon transgene (**b**). Linear map of pLV-ω1X1 showing position of regulatory
872 and coding regions for CRISPR/Cas9 editing; the positions of human U6 promoter to drive ω1
873 gRNA, translational elongation factor EF1-α promoter driving Cas9 from *Streptococcus*
874 *pyogenes*, and the left and right long terminal repeats of the lentiviral vector derived from HIV-1
875 (**c**).

876 **Figure 2. Programmed chromosomal break at ω1 locus repaired by homologous**
877 **recombination from donor template.** Schematic diagram to indicate positions of primer
878 binding sites (blue arrows), with the foreign gene cassette as the forward primer (Smω1X1-6-
879 stop codons cassette-F) paired with three discrete reverse primers, Smω1-R1, Smω1-R2 and
880 Smω1-R3 from the ω1 locus and a primer pair for target amplicon NGS library amplification;
881 miSeq-F and miSeq-R (**a**). The control PCR amplicon was generated using the Sm**ω**1-control-F
882 and –R primers. The green box shows the location of 5' and 3' homology arms, the red box and
883 arrow indicate the stop codon bearing transgene. **b**, PCR products visualized in ethidium
884 bromide-stained agarose gel demonstrating Cas9-catalyzed target site-specific insertional
885 mutagenesis in exon 6 of the ω1 gene. Evidence for transgene knocked-in into programmed
886 target site revealed by amplicons of the expected sizes in lanes R1, R2 and R3, of 184, 285 and
887 321 bp, respectively (arrows at left) spanned the mutated site in the genomic DNAs pooled from
888 schistosome eggs, including a positive control flanking the insert site (991 bp). The control
889 DNA result shown in this gel was isolated from heat-inactivated-pLV-ω1X1 virions and ssODN
890 treated LE. Similar findings were obtained when programmed gene editing was executed by
891 lentiviral virion-delivered Cas9 and ω1-gRNA transgenes and by ribonucleoprotein complex
892 (RNP) delivered by square wave electroporation (supporting information). The non-KI control
893 groups (sgRNA only, heat-inactivated pLV-ω1X1 virions only, ssODN only) showed no
894 amplicons by stop cassette-KI primers with R1, R2 or R3 (Fig. s3). **c**, Multiple sequence
895 alignments confirmed the presence of the 24 nt transgene inserted precisely into exon 6 of ω1
896 locus from KI-R1, -R2 and -R3 fragments compared with ω1 wild type (WT). The white box on
897 ω1-WT indicates the absence of the transgene sequence and white boxes on KI-R1, -R2 and –R3
898 fragments show locations of substitutions relative to the other ω1 copies (Smp_184360): 2 bp
899 (AT to CC) mismatches at positions 253-254 nt. All three contained the (knock-in) insertion
900 sequence (white box), which confirmed targeted mutation of the ω1 gene. **d-f**, Illumina deep
901 sequence analysis of amplicon libraries revealed Cas9 induced on-target repair of programmed
902 gene mutation of the ω1 locus by deletions, insertions, and substitutions by CRISPResso
903 analysis. **d**, Frequency distribution of position-dependent deletions and of deletion sizes; these
904 varied from point mutations to >20 bp adjacent to the DSB. The dotted line indicates the
905 predicted position of the programmed double stranded break. **e.** Frequency of frameshift versus
906 in-frame mutations reported by CRISPResso**.** The pie charts show the fraction of all mutations

907 (indels and substitutions) in the coding region (positions 42-179) of the amplicon predicted to
908 induce frameshifts, *i.e.* indels of 1-2 bp, or multiples thereof. Top graph corresponds to sample 2
909 (eggs only control) (Table s3), bottom graph corresponds to sample 9 (eggs exposed to virions
910 and ssODN, i.e. CRISPR/Cas9-treated) (Table s3). Findings for control and treated samples are
911 provided in Table S3. **f.** Insertions of the knock-in sequence. Number of amplicon reads
912 containing an insertion of the knock-in sequence (with ≥75% identity to it) is shown in the Y-
913 axis, and the position of the insertion relative to the reference amplicon is shown on the X-axis.
914 The programmed Cas9 scission lies between positions 102 and 103. Samples 3, 7 and 9 are
915 independent amplicon libraries (technical replicates) made from the same sample of genomic
916 DNAS pooled from six biological replicates exposed to virions and ssODN. The insert shows a
917 sequence logo, created using WebLogo (94), of the sequences of the 3,826 sequence reads from
918 samples 3, 7 and 9, with insertions of 24 bp at position 102; most matched the donor template,
919 TAAGTGACTAGGTAACTGAGTAGC.

920 **Figure 3. Diminished ω1-specific transcript levels and ribonuclease T2 activity following**
921 **programmed editing.** Panel **a,** ω1 mRNA abundance was reduced up to ~ 70% after genome
922 editing by sgRNA/Cas9 complex and lentivirus systems, and markedly reduced >80% with the
923 addition of ssODN as the DNA repair donor. Relative expression of *ω1* transcripts at three days
924 following CRISPR/Cas9 manipulation; mean ±SD, n =11 (biological replicates); $p \leq 0.0001$
925 (****) (ANOVA). **b,** Stable reduction of *ω1* transcripts at days 5 and 7 after treatment (three
926 biological replicates) in four experimental groups; RNP (black), RNP and ssODN (red), pLV-
927 ω1X1 virions (green), pLV-ω1X1 virions and ssODN (blue) compared to controls. **c,** Loss of
928 RNase activity as assessed by hydrolysis of yeast RNA. Residual yeast following exposure to
929 SEA, visualized after gel electrophoresis; lane 1, buffer (negative control); 2, RNase A; 3-8, WT
930 SEA and other control SEAs as indicated in D; 9-12, Δω1-SEA from RNP, RNP and ssODN,
931 pLV-ω1X1 virions, and pLV-ω1X1 virions and ssODN, respectively. **d,** Intact yeast RNA
932 (nanograms) remaining following incubation with SEA (mean ±SD, n = 6). More RNA remained
933 following incubation with Δω1-SEA in all groups, RNP, RNP and ssODN, pLV-ω1X1 virions,
934 and pLV-ω1X1 virions and ssODN treated SEA) (blue) than in the WT SEA controls ($p \leq$
935 0.0001). Among the gene edited experimental groups, more RNA remained when donor template
936 was introduced at the same time as RNP or pLV-ω1X1 virions ($p \leq 0.01$). Significant differences
937 were not apparent among the WT SEA control groups.

938 **Figure 4. Reduced Th2 cytokine levels following exposure to Δω1-SEA.** Reduction in Th2
939 cytokines IL-4 and IL-5 but not IL-13 (95, 96) following pulsing of Mϕ (PMA induced-THP-1
940 cells) with Δω1-SEA prior to co-culture with human $CD4^+$ T cells (Jurkat cell line) compared
941 with WT-SEA pulsed-Mϕ (top panels). In addition, levels of IL-6 and TNF-α were reduced
942 where Mϕ were first pulsed with Δω1-SEA but not WT SEA. Differences were not evident for
943 IL-10. The assay was carried out in triplicate; $p < 0.0001$, ≤ 0.0001, 0.0038 and 0.0252 indicated
944 as ****, ***, ** and *, respectively (one-way ANOVA, multiple comparison).

945 **Figure 5. Pulmonary circumoval granulomas revealed attenuated granulomatous response**
946 **to Δω1 schistosome eggs.** Schistosome eggs (~3,000 eggs) that had been transduced with
947 lentivirus virions encoding ω1-specific sgRNA and Cas9 in tandem with ssODN were introduced
948 via the tail vein into mice. The mice were euthanized 10 days later; thin sections of the left lung
949 were stained with H&E, and circumoval granulomas counted and measured. Representative 2D

950 scanned micrographs of granulomas inoculated with WT eggs (**a**) (2× magnification) and 20×
951 magnification (a1 and a2), and with Δω1 eggs; **b**, (2×), b1 and b2 (20×). **c**, Control mouse lung.
952 **d, e**, Representative micrograph of individual, control egg induced-granuloma that were counted
953 to assess for granuloma volume. **f, g**, Representative micrographs showing Δω1 egg induced-
954 granulomas. All single egg induced-granuloma from WT and Δω1 eggs were measured and
955 granuloma volume estimated (25). **h,** Scatter plots of the volume (mm^3) for individual
956 granuloma, mean ± SE (red) is shown. Granulomas induced by Δω1 eggs were significantly
957 smaller than those surrounding WT eggs (Welch's *t*-test, $p \leq 0.0001$, $n > 100$).

958

959 # Supporting Information

960 ## Supplementary Figures

961 **Figure s1. The T2 ribonuclease ω1 is encoded by at least five gene copies located on**
962 **schistosome chromosome 1.** Panel **a**. The position of several genes coding for ω1, including
963 *Smp_179960*, *Smp_184360*, *Smp_193860* are shown, to indicate the physical relationship of the
964 copies on the chromosome. Two additional copies of ω1, Smp_158430 and Smp_168300 do not
965 include the cognate sgRNA and PAM motifs. **b,** Map of gene structure and size of *Smp_179960,*
966 *Smp_184360, Smp_193860*, along with the *ω1*-specific sgRNA target site. **c,** Normalized
967 expression of three copies of ω1 as indicated throughout the developmental stages of *S. mansoni*.
968 The profile of developmental expression of ω1 was established by meta-analysis of RNAseq
969 reads (73), https://doi.org/10.1101/308213

970 **Figure s2. The nucleotide sequence** of the Smp_193860 copy, and indicates the UTR (green),
971 coding exons (blue) and introns (red).

972 **Figure s3. Variation among copies of *ω1* in the reference genome.** Panel **a**, An alignment
973 assembled using CLUSTALW (97) of the MiSeq amplicon region in the *ω1* genes *Smp_179960*,
974 *Smp_184360*, *Smp_193860* and *Smp_168300* using the sequences from the *S. mansoni* genome,
975 assembly V5. The MiSeq primers (highlighted in blue) and sgRNA (red) were designed based on
976 *Smp_184360*. Residues highlighted in green show where *Smp_168300* differs from the other
977 three genes. **b**, An alignment made using CLUSTALW (97) of the coding region of the amplicon
978 sequence found in the gene *Smp_193860* in the *S. mansoni* V7 assembly, the predicted
979 alternative sequence for the variant having 'TT' at position 60-61 and 'TA' at 152-153 in the
980 amplicon ('var'), and the translations of two mDNAs retrieved from NCBI (top BLASTP hits in
981 the NCBI protein database). Note that this corresponds to a part only of the **ω1** T2 ribonuclease.
982 The CAS-2 catalytic region is highlighted in red (29). The mRNA XP_018647488.1 has an
983 alternative splicing event at the start of the exon included in the amplicon (shaded grey), so that
984 it only matches the region from 'KHEFEK…' (in the CAS-2 catalytic region) onwards. **c**, An
985 alignment of the coding region of the amplicon sequence in schistosome ω1 homologues (family
986 873078) (40), excluding diverged members from *S. japonicum* as well as the diverged *S.*
987 *haematobium* gene *B_00112*. The region with sequence similarity to the alternative splice-form
988 is in shaded grey. Note that the *Smp_193860* sequence used in this alignment is the version in the
989 *S. mansoni* V5 gene set, which has the Q->K substitution at 152-153.

990 **Figure s4**. **Programmed HDR-catalyzed knock-in of transgene into ω1, exon 6.** The PCR
991 products visualized in ethidium bromide-stained agarose gel demonstrated Cas9 catalyzed target
992 site-specific insertional mutagenesis in exon 6 of the ω1 gene. The 24 nt transgene knocked-in
993 into target site indicated in lanes R1, R2 and R3 of 321, 285 and 184 bp, respectively (arrows at
994 left) spanning the mutated site in the genomic DNAs pooled from schistosome eggs, including a
995 positive control flanking the insert site (991 bp). Lanes 1-5 show the amplicons from the control
996 groups; medium only, sgRNA only, cas9 only, ssODN only and heat-inactivated pLV-
997 ω1X1+ssODN. Lanes 6-9 show the amplicons from experiment groups; RNP, RNP and ssODN
998 (KI), pLV-ω1X1virions, and pLV-ω1X1virions and ssODN (KI). Programmed knock-in was
999 detected only in the KI experimental groups, as shown in lanes 7 and 9 where the transgene-

1000 specific amplicon obtained with the R1, R2 and R3 primers was present. This product was not
1001 seen in PCRs where DNAs from control and other experimental groups were amplified.
1002 Amplicons of 991 bp were seen with all genomic DNAs, confirming the integrity of the genomic
1003 DNAs and the control amplicon primer pair.

1004 **Figure s5. Quantitative PCR to estimate efficiency of programmed mutagenesis**. Panel **a.**
1005 The three primers (tri-primer set): Smω1-OVR-F (probe at gRNA, expected DSB and KI sites as
1006 red bar and arrow), Smω1-OUT-F and shared Smω1-reverse primer locations used in SYBR
1007 green-based PCR to estimate efficiency of on-target, programmed CRISPR/Cas9 gene editing.
1008 Estimation of gene-editing efficiency was determined as described (46, 47). **b,** Relative fold
1009 amplification efficiency; the ratio of OVR:OUT (gray bar) was set at 100% for control DNA
1010 sample, and little or no reduction was observed in relative fold amplification compared to other
1011 control groups, including groups exposed to culture medium only, sgRNA only, Cas9 only,
1012 ssODN only, heat-killed pLV-ω1X1 virions and ssODN. By contrast, there was reduced relative
1013 fold amplification of 2.5%, 6.9%, 4.5% and 12.5% in the experimental groups, RNP, RNP and
1014 ssODN, pLV-ω1X1 virions, and pLV-ω1X1virions and ssODN, respectively. Percentages of
1015 relative fold amplification differed significantly among control and experiment groups. Means ±
1016 SE were established from six biological replicates.

1017 **Figure s6. Estimated relative copy number of *ω1*.** Copy number estimated by qPCR in
1018 genomic DNAs isolated from CRISPR/Cas9-treated eggs or controls. The relative copy number
1019 of the calibrator sample a = 1. Means ±SD: a, eggs; b, eggs and Cas9; c, eggs and ssODN; d,
1020 eggs and heat-inactivated pLV-ω1X1 virions; e, eggs, heat-inactivated pLV-ω1X1 virions and
1021 ssODN; f, eggs and pLV-ω1X1 virions; g, eggs, pLV-ω1X1 virions and ssODN.

1022 **Figure s7. Levels of IL-2, IL-10 and IFN-γ following exposure to Δω1-SEA.** Levels of IL-2
1023 (blue circle) and IL-10 (black square) were not significantly different among groups after pulsing
1024 the Mϕ (PMA-induced THP-1 cells) with Δω1-SEA prior to co-culture with $CD4^+$ T cells
1025 compared with WT-SEA pulsed-Mϕ. IFN-γ (red triangle) was not detected in any of the three
1026 groups.

1027 **Supplementary Tables**

1028 **Table s1**. Putative NHEJ and HDR pathway genes in *S. mansoni*.

1029 **Table s2.** List of oligonucleotide primers**.** Nucleotide sequences and position on the schistosome
1030 *omega-1* gene; Smp_193860.

1031 **Table s3**. Frequency of knock-in sequences, indels and substitutions in Illumina sequencing data,
1032 considering the entire 202-bp amplicon (except for 25-bp at the ends, to exclude primer regions)

1033

1034 **Supplementary methods**

1035 **Estimation of mutation efficiency**

1036 We used the egg genomic DNA templates directly for qPCR as described (46, 47), with slight
1037 modification which enabled estimation of the efficiency of CRISPR-mediated mutagenesis at the
1038 target locus without the need to normalize the experimental and control template DNAs.

1039 The general approach makes use of the fact that the binding of a primer overlapping the sgRNA
1040 site was compromised in programmed mutagenized egg (LE) genome(s), resulting in delayed
1041 amplification, whereas binding of a flanking primer pair was unaffected. The 'OUT' (flanking)
1042 primer pair encompassed at least 50 bp surrounding the sgRNA binding region. The 'OVR'
1043 (overlapping) primer pair used one of the OUT primers and another primer that bound the 20 bp
1044 of the sgRNA target sequence. The 3′ side of the OVR primer bound immediately upstream of
1045 the NGG motif, as the majority of indels would be expected to affect positions -1 to -10 of the
1046 binding site (86)(Fig. 1; Fig. s5).

1047 At days 3, 5 and 7 following transfections with or without ssODN, genomic DNA was isolated
1048 from LE. Using 5 ng of DNA template, separate 20 µl OUT and OVR qPCR reactions were
1049 undertaken. Quantitative PCR was performed with SsoAdvanced SYBR Green Supermix (Bio-
1050 Rad, 172-5271) using a Bio-Rad iQ5 Real-Time PCR system, with qPCR conditions at initial
1051 95°C for 30 s, 40 cycles, 95°C for 10 s, 60° C for 20 s. Primers are listed in Table s2.

1052 The ratio of the qPCR quantification cycle values for the control OVR and control OUT primers
1053 reflected the differences in amplification of the two primer pairs on control DNA template. This
1054 might have been due to inherent differences in amplification that exist even between perfectly
1055 complementary primer pairs. In contrast, the OVR/OUT ratio in mutant DNA reflected both this
1056 difference in amplification between the primer pairs and the loss of the OVR binding site due to
1057 CRISPR-introduced indels. A comparison of the OVR/OUT quantification cycle ratios of control
1058 versus mutated genomes thus reflected the efficiency of mutagenesis.

1059 The CRISPR efficiency was calculated by the Ct ratio of OVR:OUT, after which
1060 indel/substitution mutation percentage was estimated as follows:

1061 $$\% \text{ Relative fold amplification} = 100 \times (B/A)$$

1062 A = Ct ratio of OVR:OUT from control group

1063 B = Ct ratio of OVR:OUT from experiment group

Figure 1

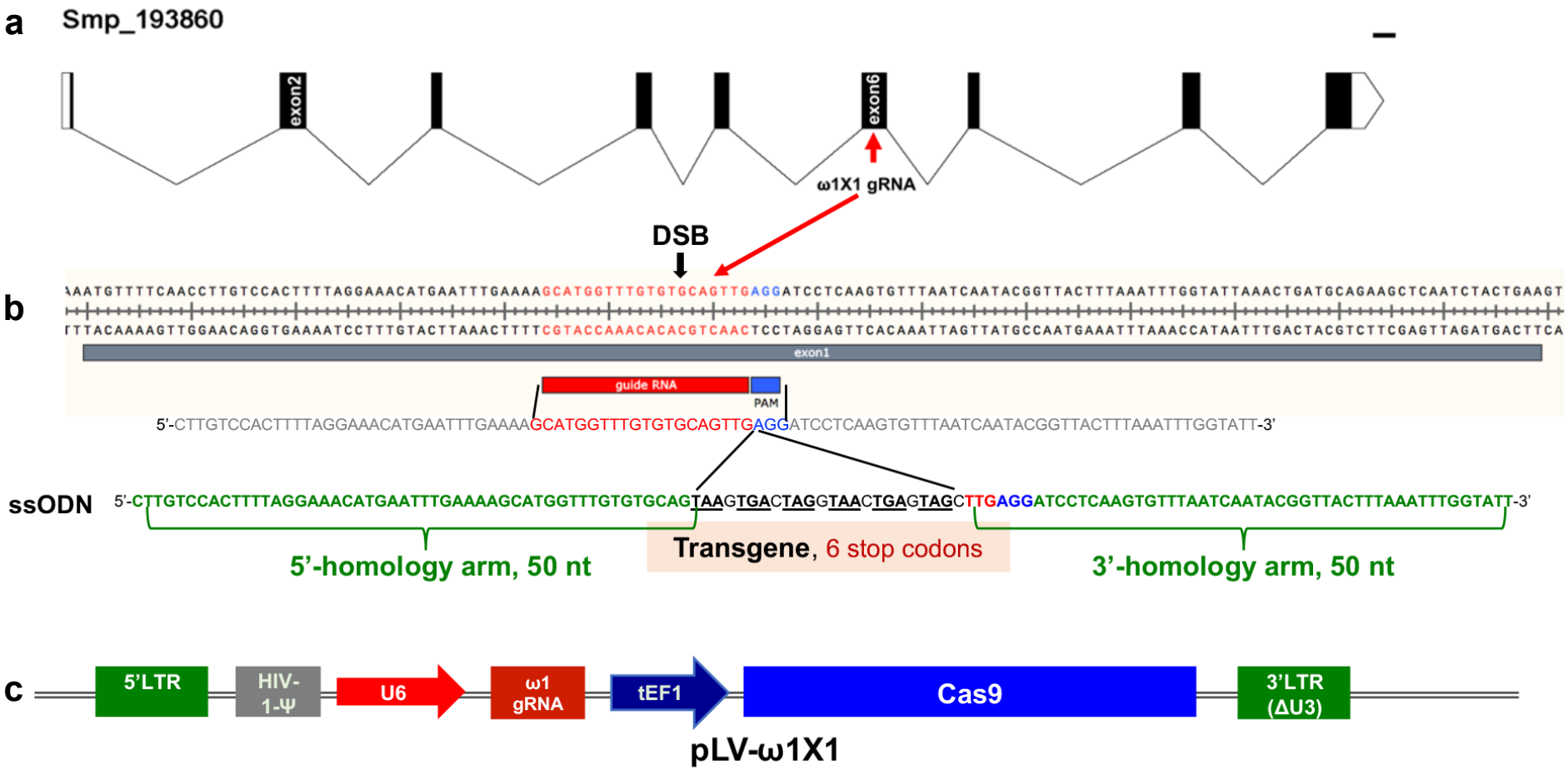
a
Smp_193860
exon2
exon6
ω1X1 gRNA
DSB
b
exon1
guide RNA
PAM
5'-CTTGTCCACTTTTAGGAAACATGAATTTGAAAAGCATGGTTTGTGTGCAGTTGAGGATCCTCAAGTGTTTAATCAATACGGTTACTTTAAATTTGGTATT-3'
ssODN
5'-CTTGTCCACTTTTAGGAAACATGAATTTGAAAAGCATGGTTTGTGTGCAGTAAGTGACTAGGTAACTGAGTAGCTTGAGGATCCTCAAGTGTTTAATCAATACGGTTACTTTAAATTTGGTATT-3'
5'-homology arm, 50 nt
Transgene, 6 stop codons
3'-homology arm, 50 nt
c
5'LTR
HIV-1-Ψ
U6
ω1 gRNA
tEF1
Cas9
3'LTR (ΔU3)
pLV-ω1X1

Figure 2

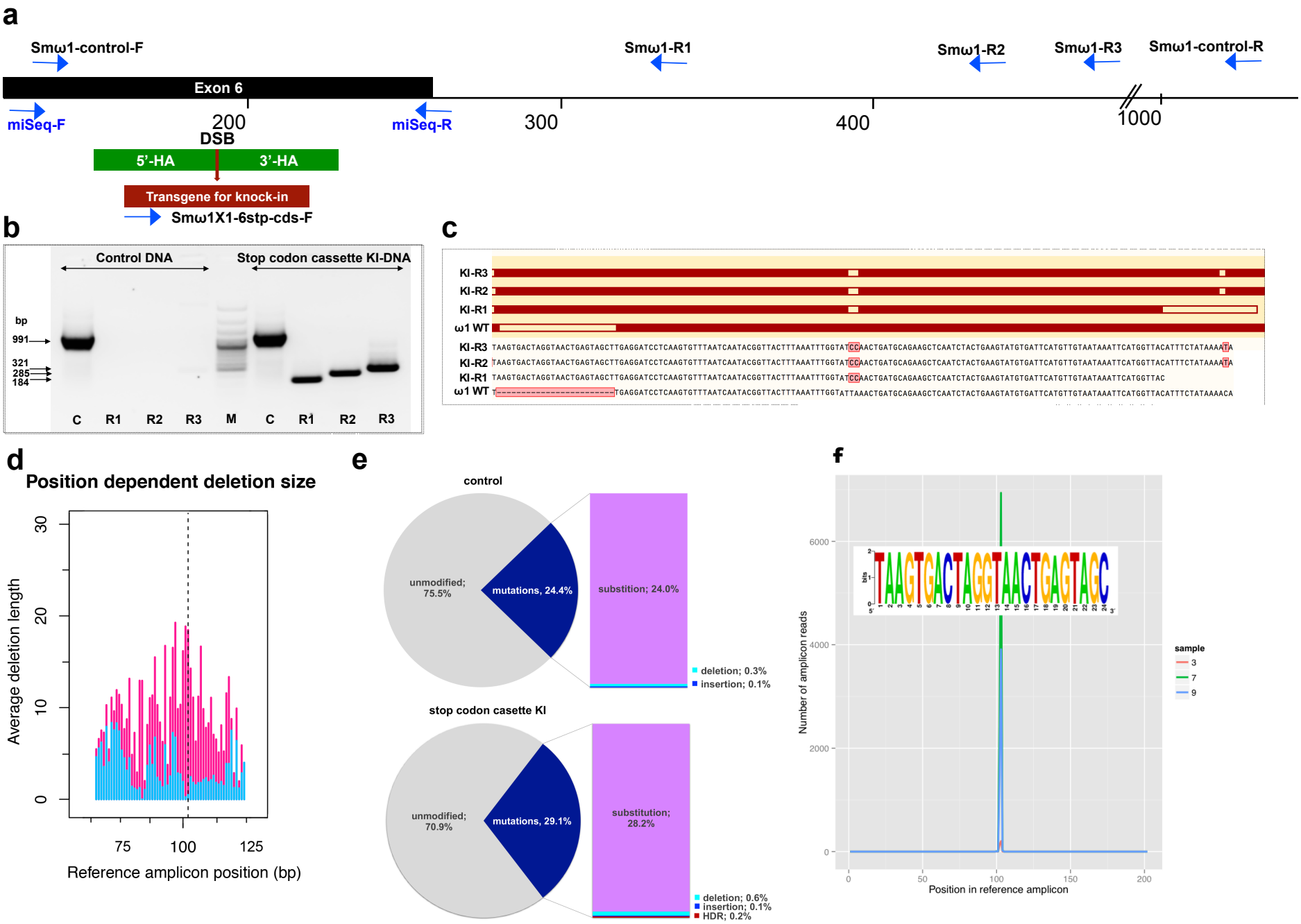
a
Smω1-control-F
Smω1-R1
Smω1-R2
Smω1-R3
Smω1-control-R
Exon 6
miSeq-F
miSeq-R
200
300
400
1000
DSB
5'-HA
3'-HA
Transgene for knock-in
Smω1X1-6stp-cds-F
b
Control DNA
Stop codon cassette KI-DNA
bp
991
321
285
184
C
R1
R2
R3
M
C
R1
R2
R3
c
KI-R3
KI-R2
KI-R1
ω1 WT
d
Position dependent deletion size
Average deletion length
Reference amplicon position (bp)
e
control
unmodified; 75.5%
mutations, 24.4%
substition; 24.0%
deletion; 0.3%
insertion; 0.1%
stop codon casette KI
unmodified; 70.9%
mutations, 29.1%
substitution; 28.2%
deletion; 0.6%
insertion; 0.1%
HDR; 0.2%
f
Number of amplicon reads
Position in reference amplicon
sample
3
7
9

Figure 3

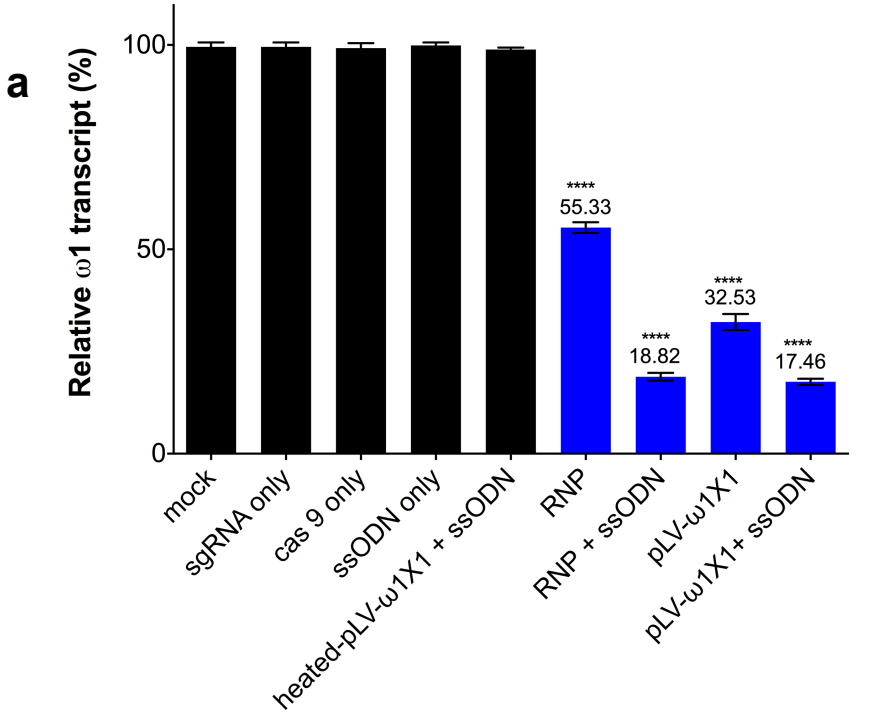
a
Relative ω1 transcript (%)
100
50
0
****
55.33
****
18.82
****
32.53
****
17.46
mock
sgRNA only
cas 9 only
ssODN only
heated-pLV-ω1X1 + ssODN
RNP
RNP + ssODN
pLV-ω1X1
pLV-ω1X1+ ssODN

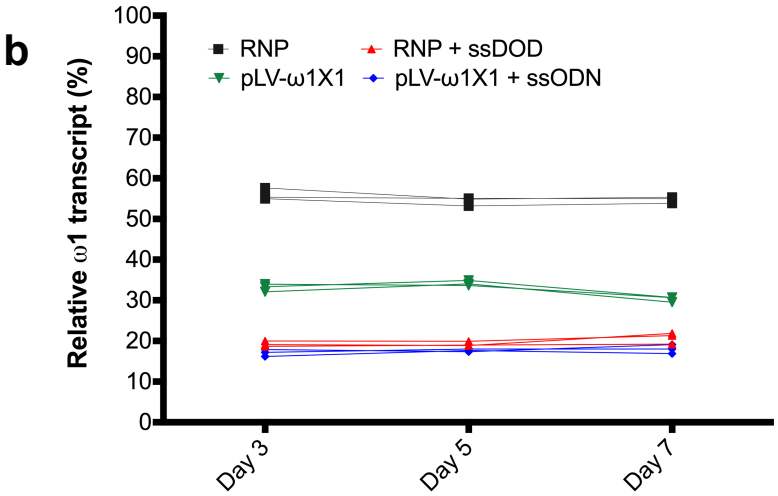
b
Relative ω1 transcript (%)
RNP
RNP + ssDOD
pLV-ω1X1
pLV-ω1X1 + ssODN
100
90
80
70
60
50
40
30
20
10
0
Day 3
Day 5
Day 7

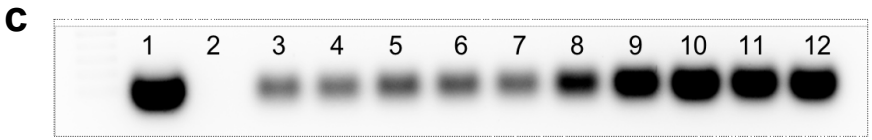
c
1
2
3
4
5
6
7
8
9
10
11
12

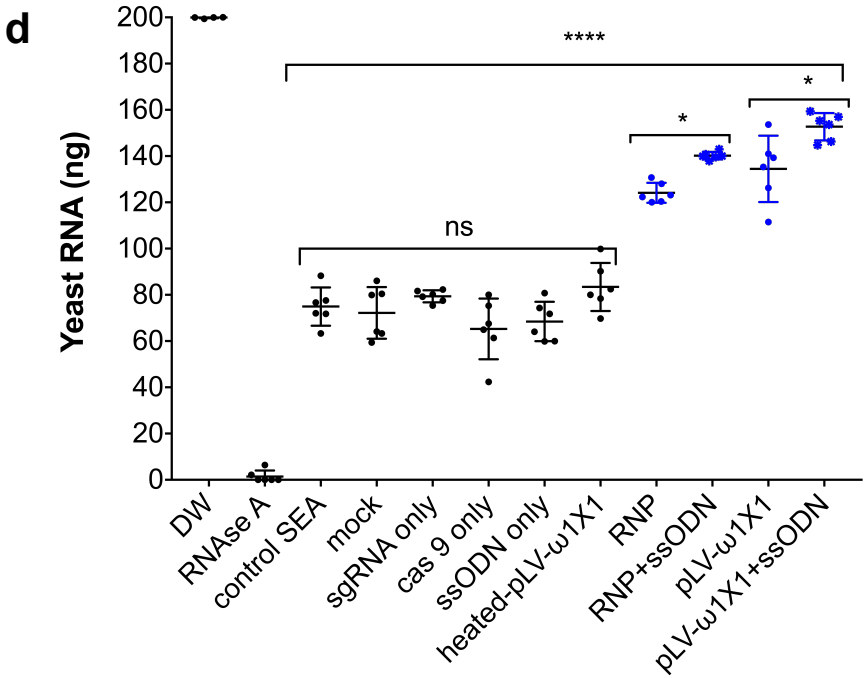
d
Yeast RNA (ng)
200
180
160
140
120
100
80
60
40
20
0
****
*
*
ns
DW
RNAse A
control SEA
mock
sgRNA only
cas 9 only
ssODN only
heated-pLV-ω1X1
RNP
RNP+ssODN
pLV-ω1X1
pLV-ω1X1+ssODN

Figure 4

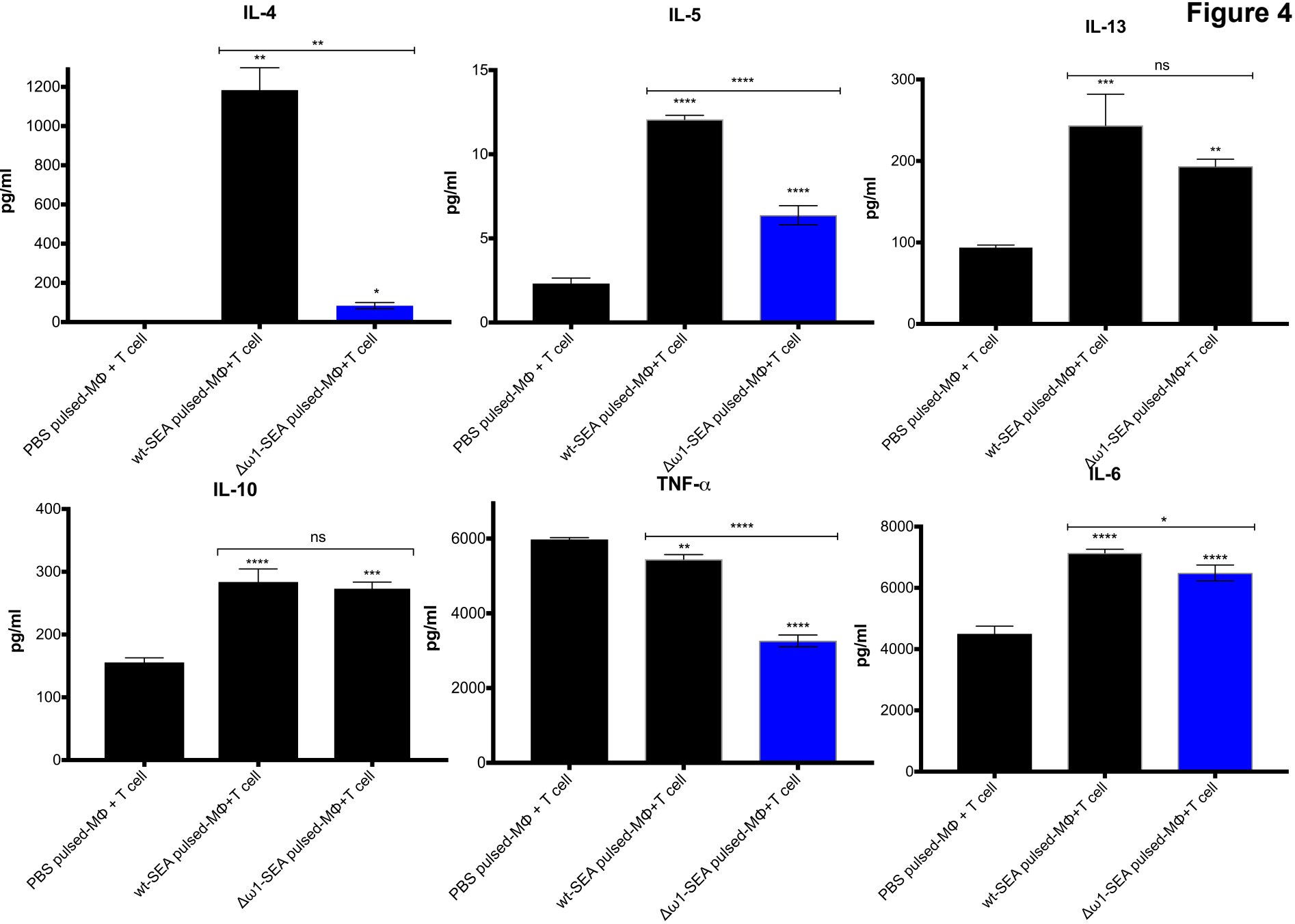
IL-4
pg/ml
0
200
400
600
800
1000
1200
**
**
*
PBS pulsed-Mφ + T cell
wt-SEA pulsed-Mφ+T cell
Δω1-SEA pulsed-Mφ+T cell
IL-5
pg/ml
0
5
10
15
****
****
****
PBS pulsed-Mφ + T cell
wt-SEA pulsed-Mφ+T cell
Δω1-SEA pulsed-Mφ+T cell
IL-13
pg/ml
0
100
200
300
ns
***
**
PBS pulsed-Mφ + T cell
wt-SEA pulsed-Mφ+T cell
Δω1-SEA pulsed-Mφ+T cell
IL-10
pg/ml
0
100
200
300
400
ns
****
***
PBS pulsed-Mφ + T cell
wt-SEA pulsed-Mφ+T cell
Δω1-SEA pulsed-Mφ+T cell
TNF-α
pg/ml
0
2000
4000
6000
****
**
****
PBS pulsed-Mφ + T cell
wt-SEA pulsed-Mφ+T cell
Δω1-SEA pulsed-Mφ+T cell
IL-6
pg/ml
0
2000
4000
6000
8000
*
****
****
PBS pulsed-Mφ + T cell
wt-SEA pulsed-Mφ+T cell
Δω1-SEA pulsed-Mφ+T cell

Figure 5

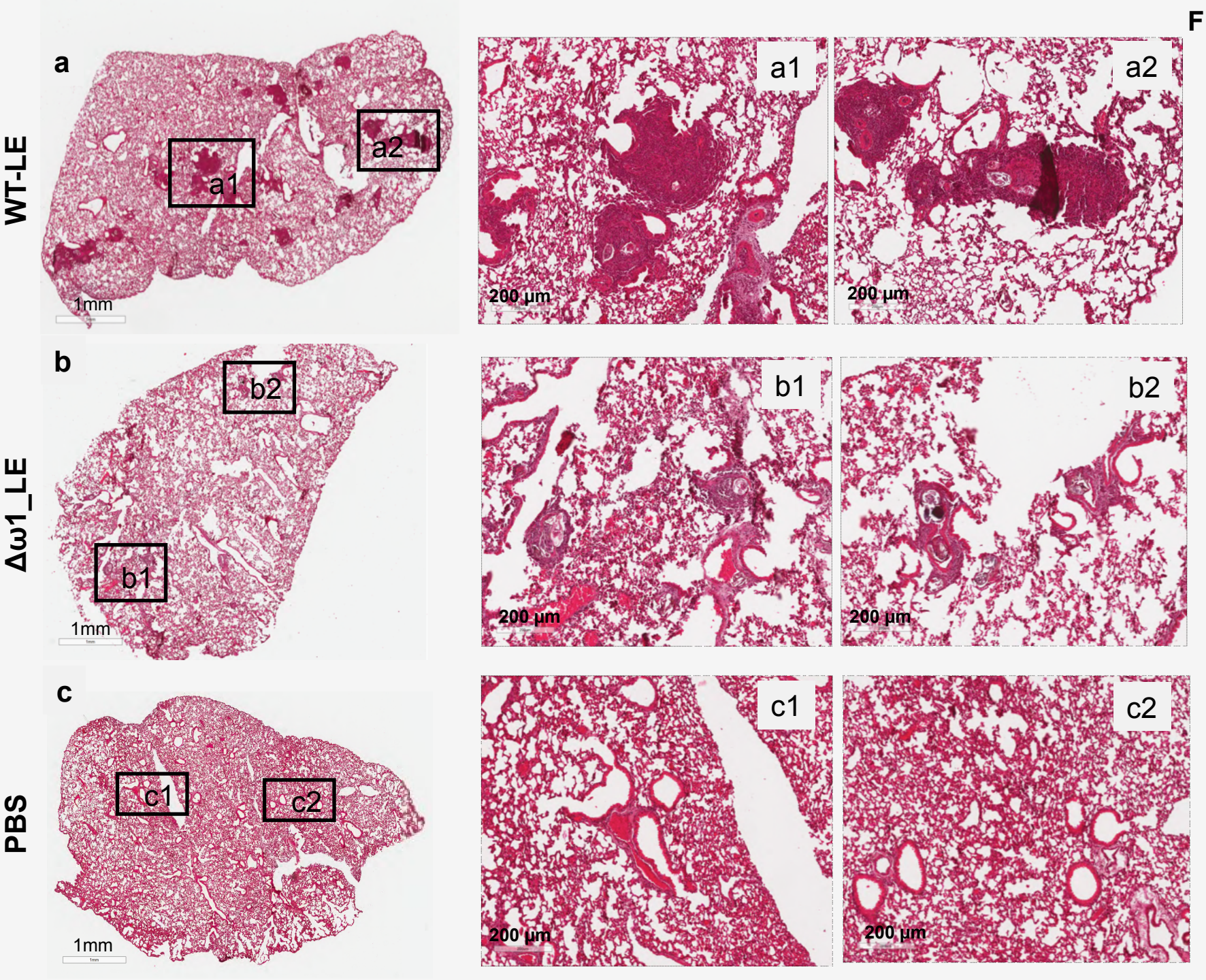
WT-LE
a
a1
a2
1mm
200 µm
200 µm
Δω1_LE
b
b2
b1
1mm
200 µm
200 µm
PBS
c
c1
c2
1mm
200 µm
200 µm

Figure 5 (cont.)

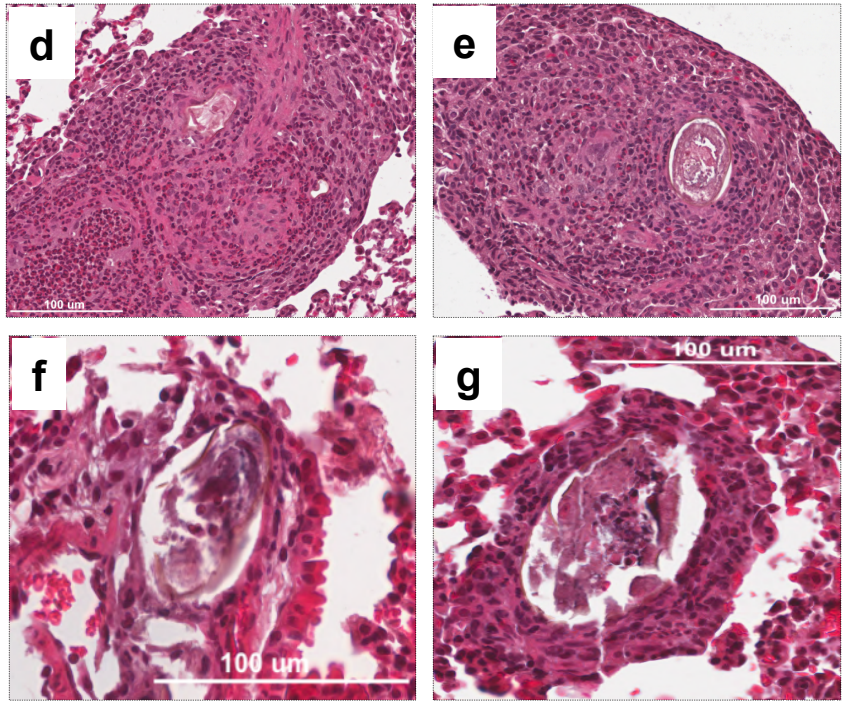

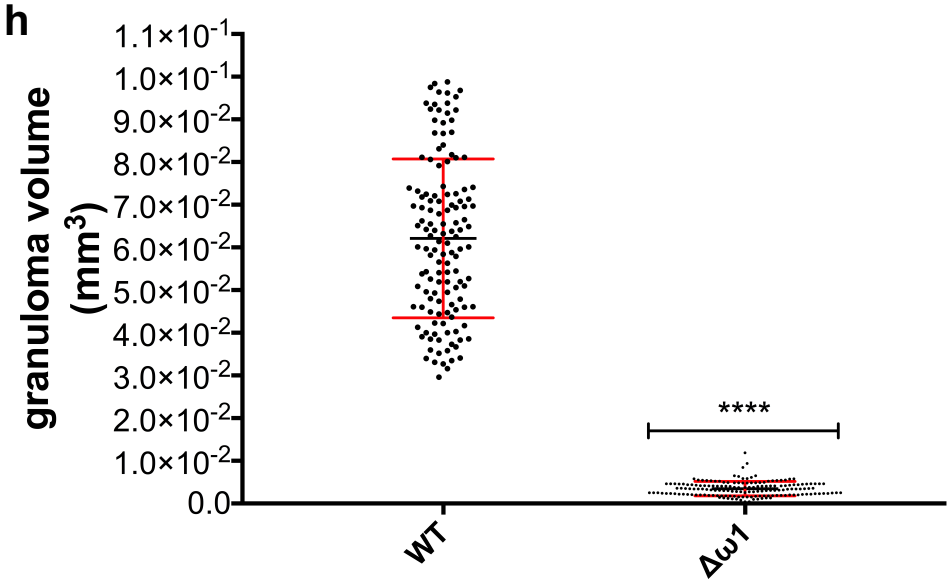

Figure s1

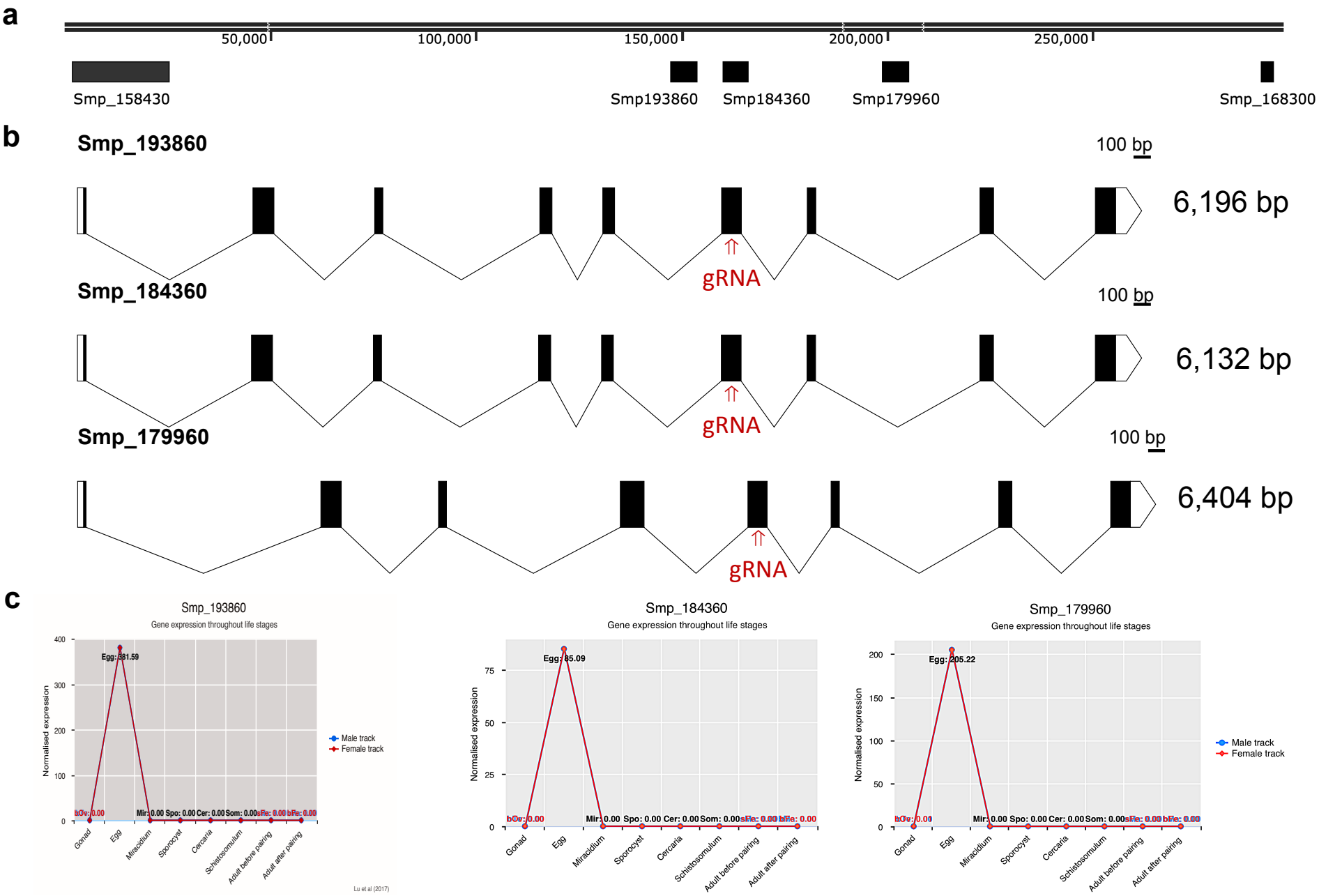
a
50,000
100,000
150,000
200,000
250,000
Smp_158430
Smp193860
Smp184360
Smp179960
Smp_168300
b
Smp_193860
100 bp
6,196 bp
gRNA
Smp_184360
100 bp
6,132 bp
gRNA
Smp_179960
100 bp
6,404 bp
gRNA
c
Smp_193860
Gene expression throughout life stages
Egg: 381.59
Normalised expression
Male track
Female track
Gonad
Egg
Miracidium
Sporocyst
Cercaria
Schistosomulum
Adult before pairing
Adult after pairing
Lu et al (2017)
Smp_184360
Gene expression throughout life stages
Egg: 85.09
Smp_179960
Gene expression throughout life stages
Egg: 205.22

Figure s2

```
ACTCAGTTATCACAATACATCAACTGATTTGGATTGATGATGAGAGCACAGTGAGTTGACGTCTTGATTTTAATGCCTGTTTGACGAGGACTATTGTCTGAGAATTAGGTGAAAGTGATAAAGCCTTCATTATATCAAGGATGAATAGCCAGCTGTTGCTATCTACAGACAAAATTGTCA 180
AATAATCTCTACCGCATTACTTTTGTTGATTGACTTTGTTTTCCTCTTGATTCAATAATTGACTGAATAAATTTATTTATGGGTTATATGTGACACCGATATTTGTCAGAACAGTGAAGTCTTCGCTAAGTATTCTGTTGATGGACGTAATTATTCTAATTACAATGAGTTTCGGCGTTT 360
AACCAATTGTTTTAGGGAGAAACAGTTGGCCAAATGTTAATCGGTTGTGTAAACTCTCAGGAATATCGTTCATGTTTCTTCGAAGTAGATGAGTGATTTGCAGAACTCACATAGTAAAAATTGTTATTGCATATAACTGCTGAGCTCCCACAATAAACAGATGAGTTGAACATTACTGAT 540
AAACATGATAGTAGCTTCACATAAAAGTTGACGAAATGTGTTCCATGTCTGTGGTCATGAGAGCTGAGCTGAAAAATCGGAAATATGAATTCTACCAGTAGTAGTAGTAGTAGTAGTAGTAGTAGTAGTAGTGCAGTAGTAGTGGTTGTTTTTAAATATTCGGAACGCTTATTGAGATAA 720
GAACTAGAAGAATGCTCACGTCAAAGAAATGCTTTACGGATTGTTTGAGATTAAATTGTATGCCGTGGCTCGTAGAAACACTGACATTAGTTACTGCACCACGTTGTTATTGCACTGCATCCTACGGCTAATCATCATCCATCTCTGCATATAAAGCATACTTGTTTTCATTAATATGAA 900
GACGTGATGATTTATTTCCCTTATCCCGGCAATGGTCTTCGTATTTCTTAAGGATGTGTTTTGCTCTTCATCGATCATGTTATTTGTGTATTGTTTACAGGTCACTCTGTTTCCTGGTGTCAATACTTGTAACCATCCTTCATGTAGGATACAGTCAAAACAGGTGGGACTACTACGTAT 1080
TTTCGGTGACTTGGCCGCCAACGTATTGTGAATCTATTCAAGTAATAAACATTTCGTATACTTAAAATGTTGTCCTTTTACATGATCTTAAACCCATCTATTCACATTTTACAGATGAATTTTATTAAGTAATATATTGTGAAATCAGTGTTTACCATTTTTCCGTTGGTGGATATGGAT 1260
CAGAGTCATTCGCTGATCGCGTACTCACCATTGTGCTATTCATTGACAGGTTGTACTCAGGGAAGTTGGGGTCAAATTACATCTTGTTAAGACATTACTTTATTTCACCAAACATGGAACTTCCAACTGTATATCATTTGCATTGAACTAGGACAATTCGACAAATCACTCTCACAGATT 1440
GCTTGAAATTGTAAACCATTTCAATCAATTTAGTAGATGTGCAATCATATTGTCCGTGTTCAGGTCTATTATGTTGGTAATGTGAAGTAATGTGAAGTTCATATCAAGGGTCAGTTTGTGAAGGTAACTAACTGAAACTACCTATTTCACTTCTAAAATTTATCTAGTCACTGGAATCGC 1620
ATTTGATAAGCCTCAGCACATATTATGTTCACATACATCTCTGTCCAACTGAGTAACAATTATTTGAAATTCTCTCTTTCAGTGTAGGCTACCGAGAGGATTGAGAGATTTCACCATTCATGGATTGTGGTAAGACTACTTTTGATTTATGAAAAATATACGTGCGTGATTATGATAATT 1800
TGAAGTATTTGATTGAAGTATAAACTATCAATACCAGCAATAACGCAATTTCATCAAGAAGTATTAGATGAGCAGGAACGATTGTACTGTATTTTGCATTCGAGTTAAAAACAGCCATCAATACTGAAGAATCATTGGTTCTTATAAACACCACATCCGCCACAGCTTGGATTCGAGTTT 1980
AGGTGTCTGTAATCGATTGTTCGTCTACTTAAGATCATCTTCCGTCTGTCCAACAGTGTATTACACATAGACTCTGTATTATCTAGAATGCACTGGTATGTATTAGAACTAACAACCGAAAATGGAACAGAGTCGCCGAATTCCTGGAGCTGCACACAATCATCATGCCGGATGTGAACT 2160
GAAACCACTGATATATAGATTTTGGACCACAGATTTTCCAACACTATTACAAACCACGAAATAATGTTGGAATTTCTTGTTGACGAATTCGTGTTGAATTATGAAGTGAATGCTGACCATTAACTATTGATTTTCTGCGCGCCCATACGACTAACGCGATCCAGGTTGTGGAGTCCATTG 2340
ATTTGCATCACAATACTATATGGTCTGAGTCTCACTGTTCCTAGATTCACAGTAATATATCTGACCACCGCAACAAGAATACTGCATTCCGTGTAACAGTTTGGTGTCGTTGATAAGATTTTAATGAGAACCTTTATGTACGCCTTTCCAATACTATGAGGTAATTAATTACTTCAAATG 2520
CTTCACACGTTCAACACAGGCATTATAGCTGTTTAGTGATAAGTTTGGGTGATCACGTTTCCGAAACGTACATGTCAGTGAATGGATGTTATTGTTTGATAAAGTGTAATGCATTATGTATATCATTATTTTCAGGCCTACCATTTTCCCCAATAGACAACCAAATTGTACTGGTTCGTT 2700
ACGTTTTGATATTCGACGTTTGCAGGTGAGTCAGATTCAAAGTTGAGTCATTTTAATTTTATTCTTACTACCTCCTATCGGTTGTCCGTGTGACTTCGTGTATTGATTGACTGTCTTGTGAAATTATCAAGTGAACTACTGCATCTGAATGAGCCGCTGACTGGTAGTGATTGAGTTGAT 2880
CGTCATTTGCTCAATGCAGATATTGCTGCAGTTGGATCAATTTTGGATCCACAAACGATCATTTTCACTTAGAAGAAATATTTTCTCAAGCTTACAACAATGCTGTCAACAAAAACTGGTGCCGATAAAAAATTTCAAACTCGCTTGTTTGTAATCACTGTATCGACGCAATCATTCACT 3060
GAAACCATTCTTTCAATTCATTCTGTGATTCTATTTCAGGGAATACGAAACGAACTAGATTTAATGTGGCCACATTTGAAAAACTACCGCGAATCACCCTCATTTTGGTAAGAGATCTAATAATATTTCATTCATCGAATATTTTATCCGGCGGCTTCGCAACATCTGATGTCGATTAGA 3240
CGATATAGATTTCTGACCATATTCTCCAATGTGACCGGTATTCAAAGCACACACCGTAAACGTAAACATTATTGAGAGGATGTTGACGTTTGATAGTTACTATGTTGAGATGTGTTTCCGTGATAAAACTATGCAGTGATAATATTTTGACTCGGAAAATGAACTTCAGATGAAAATGTG 3420
TGTTTTTTAAGAAGCAGAATCATCAGTGAGTAGTAATCATTTATCGTCGATATGCTTTGTTGACTGATGAGTGCGACCACAGTGGCAAGTGACTTTCTGTATCATCTCTTTGAACTGACGTTGTTATAAACTATCATATTGTCAACGGCGTACAGGTCCTGTGAATAAAACATCACACAA 3600
AAATCAACATACATATGATAAGGCGTTTTGTGCTGAATCCTAAATCTTCAGGTGATTCGAAATAGGGAACTTTCAACAATCAATAAAATCACGATGTTTGTTTTCGAAGACAGTTTTAGGTCGTTATCGTGTATTGTTCAATAACGTATAGTTAGTGTATCAAATGTTTTCAACCTTGTC 3780
CACTTTTAGGAAACATGAATTTGAAAAGCATGGTTTGTGTGCAGTTGAGGATCCTCAAGTGTTTAATCAATACGGTTACTTTAAATTTGGTATCCAACTGATGCAGAAGCTCAATCTACTGAAGTATGTGATTCATGTTGTAATAAATTCATGGTTACATTTCTATAAAATATTGTAAAG 3960
TTGTGCGTCTCAGTGCCGATTGGAAATGTAGATATCTACACTGATCACACTCACAATCCTGATCAATCCATGAAATAGACTCATCATATTCACTATGAACAGATGTGTTGTACCCTGTCAGTGGGATCCAGAATGCCATTTCCCCACTGAATCGAGGCTTATCAGTTGGTTCCATTTATC 4140
AAATTGACAGGCGCATATAATTTGATGTGTATCGGTTGATCAAACGACCATTGTCTGATTGATGTTACTGTGCAAGTGAATATTTGTTAAATTATACAACTTAATCTCGTGTCTTTGTTTCTATTTCTTTTCGATTATTTCAGAACACTAATGAAATATAAGATCTCACCACATGATTCC 4320
AGACAATATGATGTAAGTCTATTCTTCAACTGATAAATAGACTGAGAAAATAAATCAAATTTCTCGATCACACTATCATGTAGGCTCCACTATATATTTAGGTTGAGATCTCAGTTAATTCAAACATTGGGCACATCTCTCATTATGCATGAGCAGAAAGAATATGAACATAATTAAAAG 4500
GGAATATGTCATTGAATGATCAACCGTGTCAACGTTCATTATTGAATAACGAATTTCCTTTGAACTTAAGGGTGATATTTTAACATGAAAGGCTGACTCGAAGAGATAACTACTAACTGTTTGAGGTGATACAAATGCCGTATGAAATCTGTCATGGTAATCAAACATATTAGACTCATG 4680
TGATCACTGAACGAATCGAATGTCCACATCACTTGAACTGAACATAACAAGGATGTAGAACTTCGACGAACAACGGACAGTCACAGTAAATTTGTTGCTACTTTAGGCAAACCACCATTATTTCACGAAACAAAGTACACTTGAATGCTTACACTTGTGCAACAGTGAAAAATATGTTAA 4860
CTTGTTCATGTCAGGATCGATAGTTTTGAAAGCTGTTGCTTTTTCAGTAAGCTAACTGTGAAACTCTGGTAGAAGTAGTGGTAGTGGTGGTTGCATTGGTAGTAGTAGTAGTAGTAGTTGCAGTATAAATATTATCGCTATTAAATAATACAAGTAGTGTTATTAGTAGGTAGTTTTCTA 5040
TATATGTAGAGGTTAGTCTCCCCCATGTGGTCGCCTCTTTGTACCTCTACTAATTAACATCTGCTCTTGCGTCTCATATCCCCATGACTTTATTCGCAGATGTTTCTGATATCACCTCATTTTATTCGTCACCTTTATTACTTTTAATTAATAATGTTACGAAAGCATTTTGATCATCAT 5220
TCTTCATTCACATTATAAATAAACGGTCGAATTAATTTATGCAGACAATCAATTTAATGAATGTATTGGAACGTGAATTCGGTTACAATGGTTCTGCAAACTGCATCCGTAAACCAGGACGGGTAAGTGTATCAGTAATTAGTAATCCATTCCCTTACACACGTATAGAAAACACGTTTA 5400
CTTTACCATTAGACATTTCAGAATGTTGCATCACTTGCAAATGACACTTGAGTAAATTGTAGACAGGAATATAGTCAGACGATAAGTAGAGTCGATTTAAAATACTGAATTATATGAAGTGTAAAGATGGACTAACAAATCTAAACACATCCACAATACCTAACACAATATTGGGAGACT 5580
GTTGACACTAGTCAAACAATCGGTAAACGAGAAACATTGAACGGTGACTCGTGACAGATAGAGTTTTGGCCTCGTAGTGATTATGGAGCAACGTTGCCTGAACAATAATTAGATATTCGTGAAAGCGAATGCGTACATTGTAGTAATCTTACACGTCATGAGTTGGACAACAATCAGTGG 5760
ACAATCGTCATCTACGAGTCATGCACACCGTTTAGTTCTAATGAAATGTGTAAACAGACAATCGTTCTAGTATATAAAGTTTACTGAATATCTTATGTTGATTGATATATTTAGAGATGAATTTCATTCTGGACATTACCTAAATTCTATCGTTCTTTCATTTTTGTAGAGAGGGATGTA 5940
TCATCTGGAAGAGGTGCATGTTTGCTTGAATCGCAAACATGAATTCATGAACTGCCCGTTCCTTGGAAACTGTCCGAAGAAGTTCATCTTTCCTCCATTTCAGTAGTTGCATGAAGTTGTTTAATGAACGCACTGATTGACTCTGACAATAACAAAACCGTTCATGATTATTCATGTCAC 6120
GTCTGCTCCAACAAACAGAAATCCTCGTCATGAAGTTCATTTGTTCTTAACTAATAAATATACATTCGATCAACCA 6196
```

Figure s3

a

```
Smp_179960_V5     GTTATCATGTATTGTTCAA-TAACGTATAGTTAGTGTATCAAATGTTTTCAACCTTGTCC
Smp_184360_V5     GTTATCGTGTATTGTTCAA-TAACGTATAGTTAGTGTATCAAATGTTTTCAACCTTGTCC
Smp_193860_V5     GTTATCGTGTATTGTTCAA-TAACGTATAGTTAGTGTATCAAATGTTTTCAACCTTGTCC
Smp_168300_V5     ATTATCGTGTATTGTTTAAATGACATATGGTTATTGTATGAATTGTTTTCAACTGTGTTC
                   ***** ********* ** * ** *** **** ***** ** **********  *** *

Smp_179960_V5     ACTTTTAGGAAACATGAATTTGAAAAGCATGGTTTGTGTGCAGTTGAGGATCCTCAAGTG
Smp_184360_V5     ACTTTTAGGAAACATGAATTTGAAAAGCATGGTTTGTGTGCAGTTGAGGATCCTCAAGTG
Smp_193860_V5     ACTTTTAGGAAACATGAATTTGAAAAGCATGGTTTGTGTGCAGTTGAGGATCCTCAAGTG
Smp_168300_V5     TCTTTTAGGGAACATGAATTTAATAAACATGGTTTATGTGCAGTTCAGGATCCTCTGGTG
                   ******** *********** * ** ******** ********* *********  ***

Smp_179960_V5     TTTAATCAATACGGTTACTTTAAATTTGGTATCCAACTGATGCAGAA-GCTCAATCTACT
Smp_184360_V5     TTTAATCAATACGGTTACTTTAAATTTGGTATCCAACTGATGCAGAA-GCTCAATCTACT
Smp_193860_V5     TTTAATCAATACGGTTACTTTAAATTTGGTATTAAACTGATGCAGAA-GCTCAATCTACT
Smp_168300_V5     CATAATCAAACCGGTTACTTTAAATTTGGTCTTCAACTGTTTAAGGACGC-GAATCTACT
                    *******  ******************* *  ***** *  ** * **  ********

Smp_179960_V5     GAAGTATGTGATTCATGTTGTAAT
Smp_184360_V5     GAAGTATGTGATTCATGTTGTAAT
Smp_193860_V5     GAAGTATGTGATTCATGTTGTAAT
Smp_168300_V5     GAAGTATGTGATTCATTTTGTAAT
                  *************** *******
```

b

CAS-2
catalytic region

```
XP_018647488.1    NYRESPSFWKHEFEKHGLCAVEDPQVFNQYGYFKFGIQLMQKLNLL
ref ('AC'+'CC')   MFSTLSTFRKHEFEKHGLCAVEDPQVFNQYGYFKFGIQLMQKLNLL
XP_018647487.1    MFSTLSTFRKHEFEKHGLCAVEDPQVFNQYGYFKFGIKLMQKLNLL
var ('TT'+'TA')   MFSTLSFFRKHEFEKHGLCAVEDPQVFNQYGYFKFGIKLMQKLNLL
                        * ************************************
```

60-61 152-153

c

```
Smp_184360.1                    --NYRE-SPSFWKHEFEKHGLCAVEDPQVFNQYGYFKFGIQLMQKLNLL
Smp_179960.1                    --NYRE-SPSFWKHEFEKHGLCAVEDPQVFNQYGYFKFGIQLMQKLNLL
A_09387                         --NYSS-PETFWKHEFDKHGKCALQDPLIGNQTQYFKFGIDLMKKLNLL
SCUD_0001692401-mRNA-1          --NYSN-PESFWKYEFDKHGKCALQDPLVGNQTQYFKFGIDLMKKLNLL
A_09131                         --NYSS-PETFWQHEFNKHGQCALEDPLIGNQRQYFKFGIDLMKKLNLL
SMRZ_0002280401-mRNA-1          --NYSS-PESFWKHEFNKHGQCALEDPLIHGQYGYFKFGIDLMKKLRLL
SMRZ_0002205901-mRNA-1          --NYSS-PETFWKHEFDKHGKCALQDPLIHDQYNYFKFGIDLMKKLNLL
SCUD_0000805301-mRNA-1          --NYES-PESFWKHEFNRHGRCATEDPAIVNQHGYFKFGIDLMKKLHLL
SMRZ_0000997001-mRNA-1          --NYES-PESFWKHEFNRHGKCATEDPAIVNQHGYFKFGIELMKKLHLL
B_00903                         --DYSK-PESFWKHEFSKHGMCVHEDPKIKNQHGYFEFGLNLMKRFNIL
Smp_193860.1                    --MFST-LSTFRKHEFEKHGLCAVEDPQVFNQYGYFKFGIKLMQKLNLL
A_08953                         -----T-VFNFRKHEFDKHGKCALQDPLIGNQTQYFKFGIDLMKKLNLL
A_09441                         ---FFT-MFNYRKYEFDKHGKCALQDPLIGNQTQYFKFGIDLMKKLNLL
A_09325                         -----T-VFNFRKHEFNKHGQCALQDPLIGNQTQYFKFGIDLMKKLNLL
D_00377                         ---KKA-MAKFEKHEFNRHGRCATEDPAIVNQHGYFKFGIDLMKKLHLF
A_09388                         --MYST-MFIFRKHEFEKHGRCATEDPAIKNQHGYFKFGIDLMKKLNLL
Smp_168300.1                    MSSYVRRKLNNQEHEFNKHGLCAVQDPLVHNQTGYFKFGLQLFKDANLL
                                            ::**.:** *. :** : .*  **:**:.*::  .::
```

Figure s4

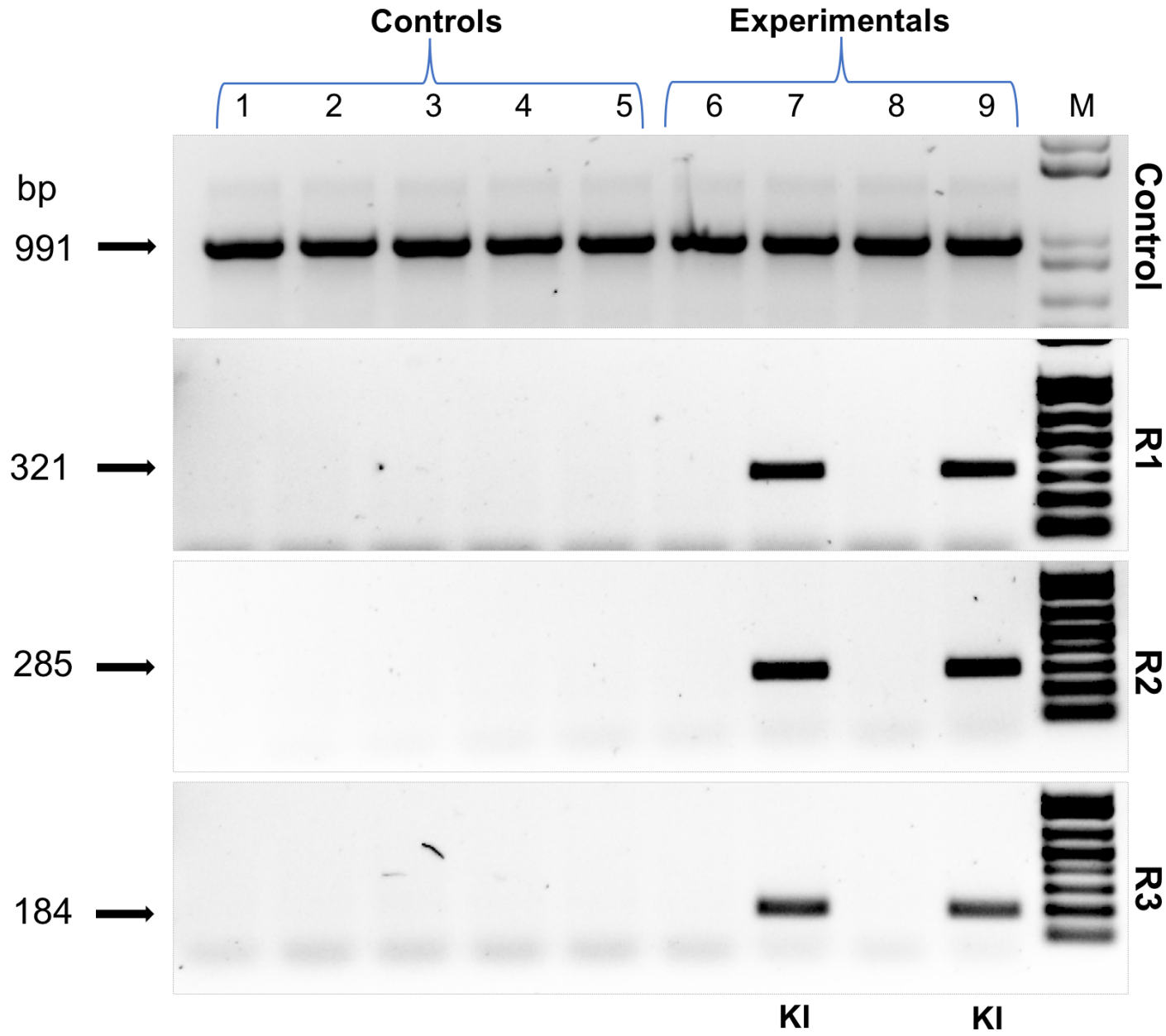
Controls
Experimentals
1
2
3
4
5
6
7
8
9
M
bp
991
321
285
184
Control
R1
R2
R3
KI
KI

Figure s5

a

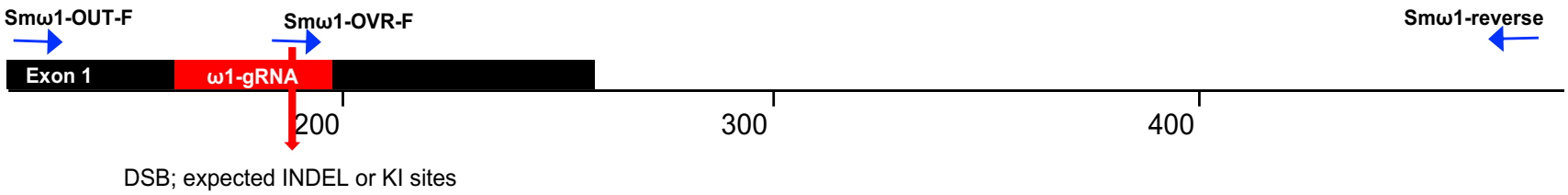
Smω1-OUT-F
Smω1-OVR-F
Smω1-reverse
Exon 1
ω1-gRNA
200
300
400
DSB; expected INDEL or KI sites

b

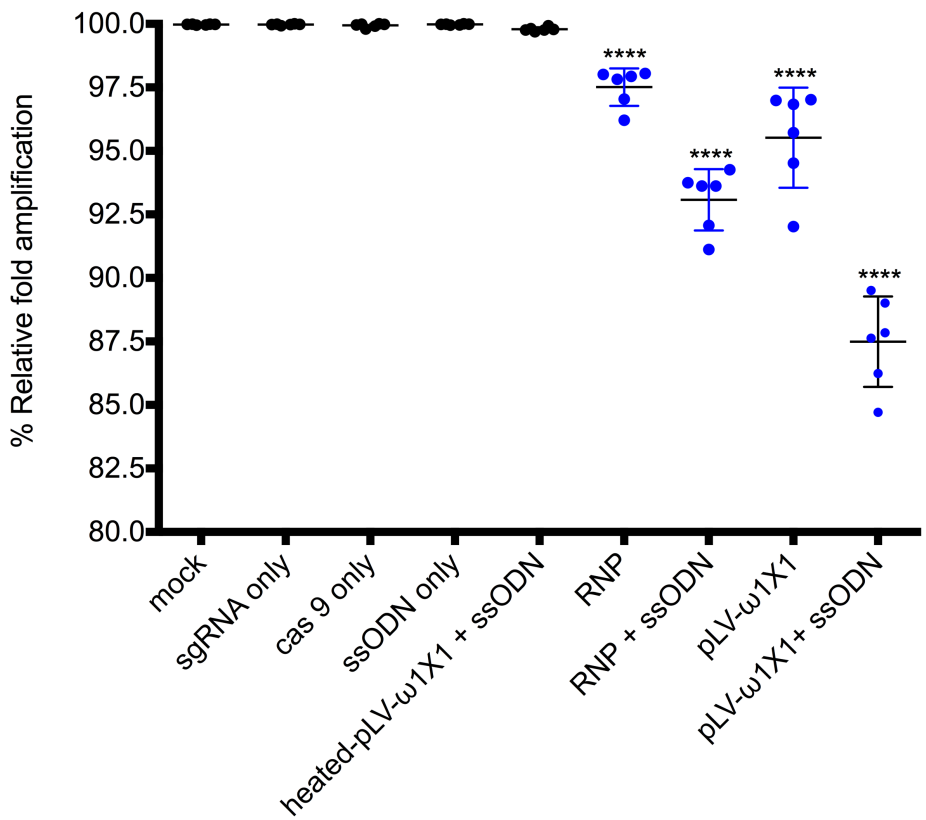
% Relative fold amplification
100.0
97.5
95.0
92.5
90.0
87.5
85.0
82.5
80.0
****
****
****
****
mock
sgRNA only
cas 9 only
ssODN only
heated-pLV-ω1X1 + ssODN
RNP
RNP + ssODN
pLV-ω1X1
pLV-ω1X1+ ssODN

Figure s6

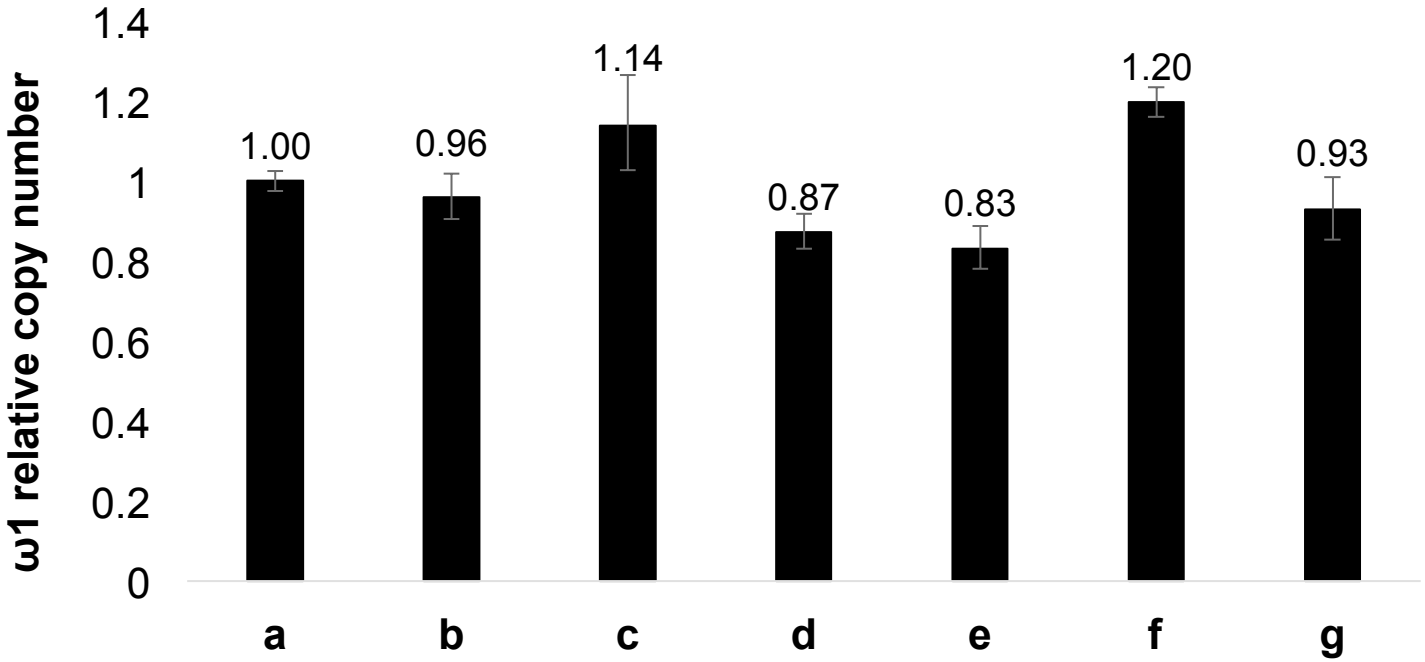
ω1 relative copy number
1.4
1.2
1
0.8
0.6
0.4
0.2
0
1.00
0.96
1.14
0.87
0.83
1.20
0.93
a
b
c
d
e
f
g

Figure s7

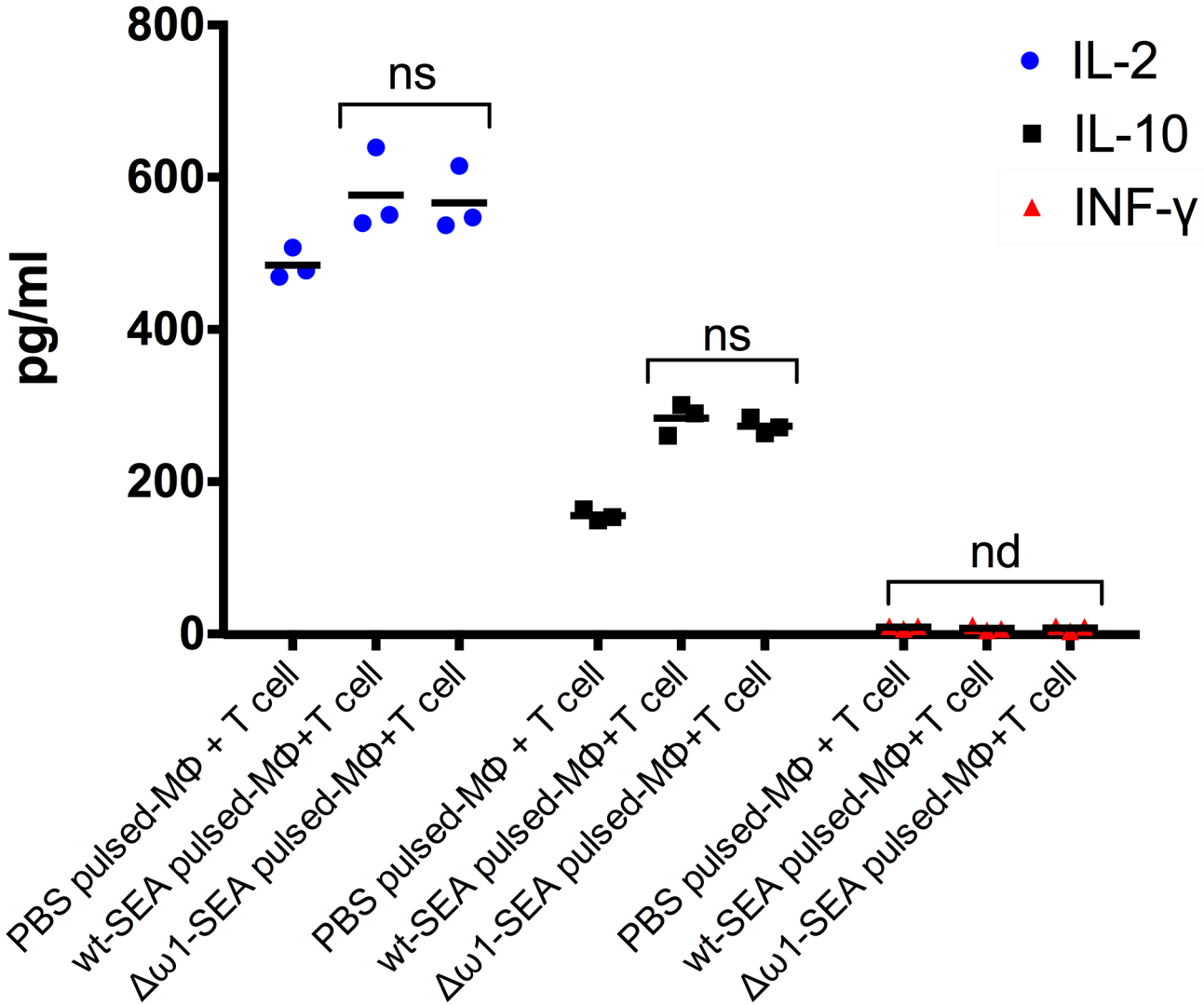
800
600
400
200
0
pg/ml
ns
ns
nd
IL-2
IL-10
INF-γ
PBS pulsed-MΦ + T cell
wt-SEA pulsed-MΦ+T cell
Δω1-SEA pulsed-MΦ+T cell
PBS pulsed-MΦ + T cell
wt-SEA pulsed-MΦ+T cell
Δω1-SEA pulsed-MΦ+T cell
PBS pulsed-MΦ + T cell
wt-SEA pulsed-MΦ+T cell
Δω1-SEA pulsed-MΦ+T cell

Table s1a. Putative NHEJ pathway genes in *S. mansoni.*

The list of human genes taken from Table 1 in Lee *et al*. (36). The Pfam domain content of *S. mansoni* genes was taken from the 50 HG data set [https://www.biorxiv.org/content/early/2017/12/20/236539]

Human gene	Ensembl/UniProt identifier of human gene	Protein domains in human gene, based on UniProt entry	*S. mansoni* genes with these domains	Best *S. mansoni* candidate
Ku70	ENSG00000196419 / XRCC6_HUMAN	Ku (PF02735) Ku_C (PF03730) Ku_N (PF03731) SAP (PF02037)	**Ku:** *Smp_211060* , *Smp_083780* **Ku_C:** *Smp_211060* **Ku_N:** *Smp_211060* , *Smp_083780* **SAP:** 6 other genes	*Smp_211060* , *Smp_083780*
Ku80	ENSG00000079246 / XRCC5_HUMAN	Ku (PF02735) Ku_C (PF03730) Ku_N (PF03731) Ku_PK_bind (PF08785)	**Ku:** *Smp_211060* , *Smp_083780* **Ku_C:** *Smp_211060* **Ku_N:** *Smp_211060* , *Smp_083780* **Ku_PK_bind:** NA	*Smp_211060* , *Smp_083780*
DNA ligase IV	ENSG00000174405 / DNLI4_HUMAN	BRCT (PF00533) DNA_ligase_A_C (PF04679) DNA_ligase_A_M (PF01068) DNA_ligase_A_N (PF04675) DNA_ligase_IV (PF11411)	**BRCT:** *Smp_148660* , 7 other genes **DNA_ligase_A_C:** *Smp_148660* , *Smp_019840* **DNA_ligase_A_M:** *Smp_148660* , *Smp_019840* **DNA_ligase_A_N:** *Smp_148660* , *Smp_019840* **DNA_ligase_IV:** *Smp_178000*	*Smp_148660* or *Smp_178000*
DNA-PKcs	ENSG00000253729 / PRKDC_HUMAN	FAT (PF02259) FATC (PF02260) NUC194 (PF08163) PI3_P14_kinase (PF00454)	**FAT:** *Smp_162340* , *Smp_122910* , *Smp_024190* **FATC:** *Smp_157820* , *Smp_142710* , *Smp_162340* , *Smp_122910* **NUC194:** NA **P13_P14_kinase:** *Smp_162340* , *Smp_122910* , *Smp_157820* , *Smp_142710* , *Smp_122910* , 5 other genes	*Smp_162340*
Artemis	ENSG00000152457 / DCR1C_HUMAN	DRMBL (PF07522) Lactamase_B_2 (PF12706)	**DRMBL:** *Smp_136360* **Lactamase_B_2:** *Smp_068090* , *Smp_031040* , *Smp_136360*	*Smp_136360*
XRCC4	ENSG00000152422 / XRCC4_HUMAN	XRCC4 (PF06632)	**XRCC4**: *Smp_135860*	*Smp_135860*
Cernunnos/XLF	ENSG00000187736 / NHEJ1_HUMAN	XLF (PF09302)	XLF: NA	NA

Table s1b. Putative HDR pathway genes in *S. mansoni.*

The list of human genes is based upon Pardo *et al*. (38). The Pfam domain content of *S. mansoni* genes was taken from the 50 HG data set [https://www.biorxiv.org/content/early/2017/12/20/236539]

Human gene	Ensembl/UniProt identifier of human gene	Protein domains in human gene, based on UniProt entry	*S. mansoni* genes with these domains	Best *S. mansoni* candidate
Rad51	ENSG00000051180 / RAD51_HUMAN, ENSG00000182185 / RA51B_HUMAN, ENSG00000108384 / RA51C_HUMAN, ENSG00000185379 / RA51D_HUMAN	Rad51 (PF08423)	**Rad51:** *Smp_124230* (e-143), *Smp_134090* (e-14), *Smp_160630* (e-6)	*Smp_124230*
RPA	ENSG00000132383 / RFA1_HUMAN, ENSG00000117748 / RFA2_HUMAN, ENSG00000106399 / RFA3_HUMAN	RFA1_HUMAN: Rep-A_N (PF04057), Rep_fac-A_C (PF08646), REPA_OB_2 (PF16900), tRNA_anti-codon (PF01336) RFA2_HUMAN: RPA_C (PF08784) RFA3_HUMAN: Rep_fac-A_3 (PF08661)	**Rep-A_N:** *Smp_121800* , **Rep_fac-A_C:** *Smp_121800* , **REPA_OB_2**: none**, tRNA_anti-codon:** *Smp_121800* and 8 others **RPA_C:** *Smp_080530* **Rep_fac-A_3:** *Smp_213370*	*Smp_121800, Smp_080530, Smp_213370*

Table s2. Primer sequences

Gene/Experiment	Name	5' to 3' sequence	Position on Smp_193860
PCR control	Smω1-control-F	GTTAGTGTATCAAATGTTTTCAACC	3751-3775
	Smω1-control-R	GTTCTACATCCTTGTTATGTTCAGT	4717-4741
6-stop codons KI test	Smω1X1-6-stop codons caset	TAAGCCTCGATTCAGTGGGG	none
	Smω1-R1	TCCAATCGGCACTGAGACG	3966-3984
	Smω1-R2	CCCACTGACAGGGTACAACA	4066-4085
	Smω1-R3	TAAGCCTCGATTCAGTGGGG	4102-4121
Amplicon miSeq library construction	miSeq-F	GTTATCGTGTATTGTTCAATAACG	3723-3746
	miSeq-R	ATTACAACATGAATCACATACTTC	3901-3924
Smω1 transcript study	Smω1-rt-F	GGTTACTTTAAATTTGGTATC	3854-3874
	Smω1-rt-R	AGTTTCCAAGGAACGGGCAG	5991-6010
CRISPR/Cas 9 efficiency primers			
	Smω1-OVR-F	GGTTTGTGTGCAGTTGAGGATCC	3812-3834
	Smω1-OUT-F	GTTAGTGTATCAAATGTTTTCAACC	3751-3775
	Smω1-reverse	GCCTCGATTCAGTGGGGAAA	4099-4118

Table s3. Frequency of knock-in sequences, indels and substitutions in MiSeq sequencing data.

The CRISPResso analysis used a window size (-w option) that included the whole 202 bp amplicon, except 25 bp at each end in order to exclude the primer regions.

Sample number	Sample	Read-pairs sequenced	Read-pairs aligned (%amplicon reads)	Unmodified amplicon reads (% of aligned)	NHEJ amplicon reads (% of aligned)	NHEJ amplicon reads with insertions (% of aligned)	NHEJ amplicon reads with deletions (% of aligned)	NHEJ amplicon reads with substitutions (% of aligned)	HDR amplicon reads reported	Mixed HDR-NHEJ amplicon reads	Confirmed knock-in amplicon reads (% of aligned)*
1	eggs + Cas9 only	5,567,790	5,450,704 (98%)	4,155,337 (76%)	1,294,899 (24%)	8751 (0.16%)	19367 (0.36%)	1287881 (23.6%)	0	468	2 (0.00004%)
2	eggs	6,145,850	6,035,043 (98%)	4,579,470 (76%)	1,455,004 (24%)	8591 (0.14%)	19624 (0.33%)	1448091 (24.0%)	1	568	8 (0.0001%)
3	eggs + pLV_ω1X1 + ssODN	6,572,305		4,949,175 (77%)	1,505,100 (23%)	10427 (0.16%)	22388 (0.35%)	1497386 (23.2%)	231	733	336 (0.005%)
4	eggs + ω1 gRNA	6,005,410	5,889,429 (98%)	4,560,750 (77%)	1,328,037 (23%)	10615 (0.18%)	19810 (0.34%)	1321434 (22.4%)	0	642	0
5	eggs + ssODN	6,203,238	6,081,763 (98%)	4,529,664 (74%)	1,569,448 (26%)	8541 (0.14%)	20692 (0.34%)	1543983 (25.4%)	0	651	3 (0.00005%)
6	eggs + heat-inactivated pLV_ω1X1 + ssODN	6,179,774	6,083,155 (98%)	4,662,311 (77%)	1,420,375 (23%)	8686 (0.14%)	19725 (0.32%)	1413041 (23.2%)	0	469	4 (0.00007%)
7	eggs + pLV_ω1X1 + ssODN	5,285,634	5,168,974 (98%)	3,744,812 (72%)	1,414,345 (27%)	5716 (0.11%)	25949 (0.50%)	1401835 (27.1%)	1	9816	9368 (0.18%)
8	eggs + heat-inactivated pLV_ω1X1	5,269,242	5,192,472 (99%)	3,942,608 (76%)	1,249,483 (24%)	6883 (0.13%)	16282 (0.31%)	1243438 (23.9%)	2	379	4 (0.00008%)
9	eggs + pLV_ω1X1 + ssODN	2,965,075	2,894,187 (98%)	2,066,129 (71%)	822,372 (28%)	3656 (0.13%)	16678 (0.58%)	814770 (28.2%)	0	5686	5419 (0.19%)
10	eggs + pLV_ω1X1	5,963,235	5,887,422 (99%)	4,415,104 (75%)	1,471,950 (25%)	6160 (0.10%)	18554 (0.32%)	1464598 (24.9%)	0	368	2 (0.00005%)

* Column I is the number of insertions of the 24-bp knock-in sequence confirmed by ggsearch, by checking for insertions that have >=75% sequence identity to the expected 24-bp knock-in sequence.